THE H-ALPHA LINE IN LATE G AND K SUPERGIANTS

S.G.V. MALLIK

Thesis submitted to the
Madurai University
for the Degree of
Doctor of Philosophy

INDIAN INSTITUTE OF ASTROPHYSICS

October 1979

Certificate from Supervisor

I certify that the thesis entitled "THE H-ALPHA LINE IN LATE G AND K SUPERGIANTS" by Mrs Sushma Gupta Mallik is a record of research carried out by her in the field of "Stellar Atmospheres" at the Kodaikanal, Kavalur and Bangalore units of the Indian Institute of Astrophysics. I declare that the thesis has not previously formed the basis for the award of any Degree, Diploma, Associateship, Fellowship or similar title. It contains an account of spectroscopic observations of late type supergiant stars made by the candidate and her inference of mass loss from these stars.

M.K.V. Bappu
Director
Indian Institute of Astrophysics.

ACKNOWLEDGEMENTS

I wish to express my deep appreciation to Professor M.K. Vainu Bappu for his supervision and wise counsel throughout the course of this work. I am also indebted to him for generous allotment of observing time. I am especially grateful to Dr. A. Peraiah for providing theoretical insights into the problem of line formation and allowing me to use his radiative transfer code. Without his code, this work would have been incomplete.

I also wish to express my sincerest thanks to Margaret Biswas for help in computing. The assistance of Mr. A. Charles at the Echellé spectrograph of the 40" telescope is gratefully acknowledged. I thank Mr. A.M. Batcha for doing an excellent job of typing the manuscript in a short time and Mr. Sampath Kumar for his services in drawing the figures. I especially appreciate the help of Mr. R. Krishnamurthy in copying all the Figures and Mr. and Mrs. Krishnamurthy for binding the thesis.

Lastly, this work would have been impossible but for the unsparing criticism and indispensable help of my husband.

This research was supported by the NCERT and the Indian Institute of Astrophysics.

TABLE OF CONTENTS

SUMMARY

A spectroscopic survey in the red has been done to investigate the properties of expanding chromospheres of late G and K supergiants. Spectra of 23 stars brighter than $m_V = 6.0$ have been obtained at dispersions of 4-10Å mm^{-1} using the coudé and the echellé spectrograph on the 40" telescope at Kavalur Observatory. In particular, the H_α line and the CaI] λ 6573 line have been studied. It is found that the H_α line profiles are all asymmetric in the sense that the absorption core is shifted to the blue by an amount ranging between -4 and -24 kms^{-1}. The CaI] absorption cores are also displaced to the blue but by a smaller amount. No clear dependence of the H_α and the CaI] line core displacements upon the spectral type has been found. Unlike the case of the Ca II K line, the H_α equivalent widths are found to be uncorrelated to the corresponding line core displacements. However, the H_α and the CaI] line core displacements are linearly correlated.

H_α line profiles have been theoretically computed using a proper radiative transfer formulation in spherically symmetric expanding atmospheres. Different sets of density and velocity distributions in the model envelope have been tried to obtain profiles that fit

best the observed characteristics of the line in the programme stars. Each theoretical profile is characterised by an optical depth, a turbulent velocity and an expansion velocity.

The analysis shows that the H_α line though unsaturated is of moderate optical thickness and is formed in a region of small geometrical extent with an increasing velocity gradient. The computed equivalent widths and the line core displacements have been matches with the observed to obtained hydrogen column densities and expansion velocities. These have been used to calculate the rate of mass loss in these stars. The derived values are in the range of 10^{-6}-10^{-7} $M_\odot$ /yr. a little higher than what Reimers' (1975) mass-loss rate formula implies.

CHAPTER I

Introduction

The study of the outer layers of supergiant stars is complicated by several factors. Firstly because of their vast extent, the classical plane-parallel atmospheres theory is not applicable to them. Only in the last few years, the theory of radiative transfer in extended and expanding atmospheres has become widely available. Therefore, until recently it was not possible to properly interpret the observational data relating to these supergiant atmospheres. Secondly, in the case of sun, the hydrogen convection zone is thought to give rise to the non-radiative flux through the photosphere. Since all stars cooler than spectral type F5 have deep convective zones where the radiative temperature gradient becomes steeper than the adiabatic temperature gradient, they should have a significant non-radiative flux at their photospheres. As a result, late-type supergiants are most likely to have chromospheres and coronae. Ca II H and K emission which is chromospheric in origin has been observed for a large sample of G, K and M giants and supergiants (Wilson and Bappu 1957, Wilson 1976). MgII h and k and FeII emission on the ultraviolet have also been detected confirming

chromospheric activity in these stars (MsClintock, Henry, Moos and Linsky 1975, Dupree 1976). Over the past couple of decades, enough observations have accumulated to also suggest that a steady outflow of mass is taking place from these stars. This adds a new dimension to the problem of supergiant atmospheres. Knowledge of the phenomenon of mass-loss is important for several reasons. From the point of view of stellar evolution the course of a star's life may drastically change if significant mass loss occurs. Even otherwise the process of mass ejection reveals the layers underlying the very outer layers of a star to the observers' view and provides a way of testing the theory of stellar evolution and studying the consequences of nuclear processing followed by extensive mixing. The matter ejected forms a circumstellar (CS) envelope around the star.

The first observational evidence of the existence of CS envelopes came from the work of Adams and McCormack (1935). They obtained spectra of the bright stars α Ori, β Ori, α Cyg, α Sco, α Her, β Peg and ϵ Peg at high dispersion at the coudé focus of the 100" telescope. They noticed that the cores of several strong resonance lines and lines arising from low-lying levels in these stars were shifted to the

blue with respect to the other lines in their spectra. The NaI D lines were found to be displaced with respect to the normal stellar lines by about 5 km/sec to the blue. The H and K lines of CaII and the lines of AlI at $\lambda\lambda$3944, 3961 also showed the same amount of displacement. However, the SiII lines were displaced by a slightly lesser amount. The interstellar origin of these displaced lines was ruled out on the basis that all the displacements were larger than what is expected, were the lines of such origin.

Adams and McCormack explained these shifts as due to the absorption of radiation from the star by a slowly expanding gaseous envelope surrounding the star. However, their discussion did not go beyond this to the suggestion of a steady outflow of mass. Nothing very significant was added in the intervening years until Deutsch (1956) rediscovered similar asymmetries on the spectrum of the spectroscopic binary α Her obtained at a dispersion of 4.5Å/mm at the 200" telescope. He observed that the lines of NaI at $\lambda\lambda$5890, 5896, CaII H and K, KI $\lambda\lambda$7665, 7698 and a few other metal lines were shifted to the voilet not only in the spectrum of the M supergiant but also in the spectrum of its GOIII companion α^2 Her. Since physical conditions in

the atmospheres of G giants are not suitable for the production of these lines, Deutsch suggested that the primary had an extremely extended outer envelope which also engulfed the GOIII companion. Deutsch demonstrated that the circumstellar envelope surrounding α Her extended to as many as a few hundreds of stellar radii. For the spectrophotometric study of circumstellar (CS) lines, Deutsch isolated the contour of the CS line from the underlying photospheric profile by referring to this underlying radiation as the effective continuum. The equivalent widths were determined and the curve-of-growth technique was used for determining the physical parameters partaining to the CS envelope. He found that the envelope expands at a moderate velocity of $\sim$ 10 km/sec. He concluded that since the 10 kms^{-1} velocity of matter was greater than the escape velocity at the edge of the envelope, the system was ejecting mass. The mass-loss rate was found to be 10^{-8} $M_{\odot}$/year. Later Deutsch (1960) made a high dispersion survey of the red-giant region of the HR diagram and found that the strongest CS lines always happened to be CaII H and K and they were present in the spectra of giants and supergiants of type M0 and later and also in many G and K supergiants. Other CS lines observed were CaI λ 4227,

Sr II λ4078, CrI λλ4254, 4275, AlI λλ3944, 3962, MnI λλ4030, 4033, 4034, FeI λλ3824, 3860, 4216. Deutsch found that the strength of the lines increased with later spectral types and with luminosity. He also found a correlation between the velocities determined from the blue shifts of the CS H and K lines and the spectral type in the sense that these expansion velocities increased as one approached the earlier spectral types. There was also a definite trend of velocity shifts decreasing with the strength of the CS lines. He suggested that the amount of matter in the envelope and/or the state of ionization of Ca largely determine the above correlations.

A very detailed analysis of CS lines in the M supergiant α Ori was undertaken by Weymann (1962). The spectra were obtained at the 100" telescope covering the range λ 3150-4900. The dispersions varied between 1 and 3Å/mm. These spectra together with the older ones taken by Adams and by Struve at 2.8Å/mm were analysed for the circumstellar studies of α Ori. The position of the line center of the photospheric component was located by measuring with respect to the neighbouring photospheric lines. The red half of the photospheric profile was then reflected around the

line center and was used as the effective continuum for the CS core component. The CS lines were next analysed with the help of the curve of growth technique. Since the densities and the level of excitation in the envelope seemed to be low, Weymann used the methods normally applied to the studies of gaseous nebulae. He assumed a constant velocity of outflow of the gas in the shell and hence the density veried as $\frac{1}{r^2}$. He also assumed that the envelope is detached from the star in the sense that no contribution to the strength of the lines came from below a certain point, a few times the stellar radius. The expansion of the envelope relative to the photosphere turned out to be $\sim$10 km/sec. He also obtained a density of 10^8 particles/cm^3, an electron density of 10^4/cm^3 and a kinetic temperature of the order of 1000°K in the CS shell. He found that the CS components in the spectrum of α Ori did not show the radial velocity variations of the underlying photospheric lines and, therefore, confirmed that the CS shell was detached from the star. His analysis gave a mass loss rate of 4×10^{-6} $M_\odot$ /yr. based on $R_* = 6.3 \times 10^{13}$ cm, V = 10^6cm/sec, N = 10^{22}/cm^2 and the distance = $10R_*$ = extent of the shell. This rate is crucially dependent upon how many stellar radii away the CS lines are formed.

Both Deutsch (1956, 1960) and Weymann (1962) based their curve of growth analysis on a plane-parallel pure scattering atmosphere. Although nothing better could be done at that time, it does seem unrealistic now to use plane-parallel atmospheres for the study of expanding CS envelopes.

Reimers (1975) using Wilson's and Deutsch's plate collections found CS absorption features in the spectra of more than 120 M type giants, bright K giants and G, K and M supergiants. From this large sample of stars, Reimers confirmed the increase of the absorption width of the CS CaII H and K lines with earlier spectral types and also the dependence of the width on the measured velocity shift of the line center. Moreover, he found that in a few early M giants the CS H and K lines are variable in velocity and strength. The shortward edge, according to him remains stationary whereas the red edge changes with time. Reimers also reported the existence of velocity gradients in the CS envelopes of G and K supergiants. He found H and K lines systematically shifted to the blue in giants and to the red in supergiants, relative to the other CS lines and attributed this phenomenon to the formation of the CaII H and K lines further out in the shell

where the matter has been accelerated to a terminal velocity plateau.

Later Reimers (1977) in his search for CS lines in stars earlier than type MO found that all stars cooler and brighter than a line in the HR diagram defined by (K5, M_v = 0.0), (K4, - 1.0), (K2, -1.8) and (G5, -4) show CaII H and K CS lines. This limit owed mainly to the second ionization of Ca. Throughout the analysis, Reimers, used plane parallel atmospheres. More recently, Sanner (1976), Bernat (1977) and Hagen (1978) have studied in detail the CS envelopes of M supergiants. They used radiative transfer in expanding spherically symmetric atmospheres to produce the CS line profiles to be fitted with their observations. In the above three pieces of work, the observed line asymmetries were treated as the modification of the underlying symmetric photospheric profile by the CS envelope. Assuming the CS envelope to be detached from the star, the observed CS line profiles were isolated from the composite line profiles using Weymann's technique. A series of theoretical CS line profiles were then computed for various line center optical depths, expansion velocities and turbulent velocities and these were matched with the observed profiles to

obtain column densities. Various physical conditions in the CS envelopes including their kinematics, state of ionization, dust content and mass loss rates were inferred from the analysis.

Sanner (1976) in his study of 13 M giants and supergiants found that the inner shell radii of giants ranged from 2 to 4 stellar radii whereas the shells of supergiants extended to about 5 stellar radii. The hydrogen densities at the inner radius of the shells varied between 5×10^6 cm^{-3} and 10^9 cm^{-3}. The expansion velocities were found to be in the range 5-15 km-sec. The mass loss rates calculated were of the order 10^{-7} $M_\odot$/yr. He found that the level of ionization did not vary much over the range of the spectral types and luminosities considered.

Bernat (1977) in a very detailed work on the circumstellar shells of four M supergiants, showed that the physical dimensions of the CS shells were very much more extended ($\geqslant 10$ R_*). As a consequence, his mass loss rates turned out to be higher, e.g., in the range $(6.7 \times 10^{-7} - 4.2 \times 10^{-4}) M_\odot$/yr.

Hagen (1978) studied nine M giants supergiants both in the optical and in the infrared region to

investigate how the presence of dust among other things might affect the physical situation in the shells. Her expansion velocities were of the same order as obtained before and particle densities of 10^7-10^8 cm^{-3} at the inner edges of the envelopes were inferred. The mass loss rates were in the range 10^{-7}-10^{-8} $M_\odot$/yr. - more like Sanner than Bernat. These values depend critically upon the value of the inner shell radius used in the calculations. Both Sanner and Hagen took a smaller value for this radius than Bernat.

With the exceptions of Sanner (1976) and Bernat (1977) who used apart from metal lines CaII infrared triplet lines at $\lambda\lambda$8498, 8542, 8662, NaI D lines at $\lambda\lambda$5890, 5896 and KI lines at $\lambda\lambda$7665, 7699 most of the analyses so far have been based on observations in the blue. This has been so primarily because most of the circumstellar lines of the abundant metals are located in the blue-violet part of the spectrum. However, these cool giants and supergiants are rather faint in the blue which restricts the observations to the very bright stars. The circumstellar cores usually fall within the wings of the underlying photospheric line. Therefore, heavily exposed spectrograms are required to reach the CS cores. This requirement further limits the selection of the objects. Unlike the CS envelopes

in M supergiants which are comparatively well studied, the observational data relating to those of late G and K supergiants are rather scanty. It may be that very few CS lines were found in the blue in G and K supergiants. Owing to the lack of knowledge of the level of Ca ionization, the CaII H and K lines are unsuitable for the accurate determination of the mass loss rates in these stars. Therefore, there is a pressing need to explore the CS lines in the red in these stars. Weymann (1962) had noticed during the course of his study of the CS spectrum of α Ori, a distinct asymmetry in the profiles of the first two Balmer lines of hydrogen. The asymmetry was much more apparent in H_α than in H_β. He suspected that these lines are formed in a massive expanding chromosphere surrounding the star. Kraft et al (1964) in their study of H_α core widths also observed that in most of the K supergiants, the H_α line was asymmetric in the sense that the deepest part of the line was shifted to the shortward edge. They also found that a few of them had small emission components lying above the level of the continuum on the blue side; for 12 Peg, the emission was observed to be on the red end. The H_α emission components superposed on the chromospheric absorption cores probably originate in the CS shells. Cohen (1976) had reported the discovery of

weak emission components of H_α in red giants in globular clusters. She interpreted these as emissions from the circumstellar shells formed by ejection of matter from these giants. Mallia and Pagel (1978) confirmed the presence of these small emission features in red giants in a few more globular clusters. The emissions are detected either on the blue edge or on the red edge or on both the edges of the H_α profiles. According to them, the blue shifts of the H_α absorption core coupled with the presence of weak emission components are highly suggestive of mass loss. Very recently, Boesgaard and Hagen (1979) have also detected small asymmetries in the H_α absorption lines in several M giants. They obtained high dispersion spectra of 61 M giants to investigate the behaviour of CaII H and K, NaI D and H lines in the CS envelope. The H_α line was found to be asymmetric in 50 per cent of the stars. The displacements from the line center measured forthe CaII H and K lines were much larger than for the H_α lines. Boesgaard and Hagen also suggested that the H_α asymmetry arises most probably in the chromosphere and that the line forming region extends over a small geometric distance. They confirmed that the strength of the CaII K component increased with the spectral types and the velocity shifts

decreased. On the other hand, the H_α core strengths and the displacements did not vary much with the spectral type.

Since H_α is a strong line in late type supergiants where the bulk of the stellar continuum is in the neighbourhood of H_α , it should be a powerful tool for the analysis of expanding chromospheres and envelopes of these stars. Because of its intrinsic strength, a larger domain of stars to fainter limits can also be studied.

The present work is undertaken to investigate physical conditions in the very outer layers of middle G to early K supergiants with the H_α line as a probe. The process of mass ejection and the physics of expanding shells of these stars are studied.

We have obtained coudé spectrograms and echellograms at high to moderately high dispersions of 22 stars ranging in spectral type from G8 to K7. The observations are designed to study the neighbourhood of the H_α line and includes in particular the [CaI] λ6572.

Series of H_α line profiles are computed with varying physical parameters to match the observed profiles. For the line profile computations, a

radiative transfer code for spherically symmetric expanding atmospheres (developed by Dr. A. Peraiah) has been used. From the fits to the observed profiles we have obtained data on the densities, velocities and physical extent of the H_α forming layers as also the mass ejection rates of these stars implied by the observed asymmetries in the H_α line and the weak emission components flanking the central absorption. We have also tested if the CaI]λ6573 could be used as an effective probe of the chromospheres and CS envelopes of these stars.

We discuss the observations and the methods of reduction in detail in Chapter II. In Chapter III the theoretical framework for the analysis of the line profiles is explained. In Chapter IV, we describe the results and discuss their implications. Conclusions and the future directions of work in this field are given in Chapter V.

CHAPTER II

Observations

a. The Programme

From the Bright Star Catalogue (Dorrit Hoffleit, 1964) and the list of supergiants given by Humphreys (1970), late G and K supergiants were sampled keeping in mind their observability from Kavalur Observatory which is at a latitude of 12° and the limitations imposed on their brightness by the duration of the exposure required at the coude and the Echellé spectrographs of the 40" telescope. Stars with declinations as low as -64° could be observed under conditions of good seeing and transparency. Since the Echellé spectrograph was used in conjunction with an uncooled single stage Varo image tube the exposure times were further limited by the ambient temperature resulting in a high background of the image tube. The observations were thus restricted to objects brighter than $M_V = 6.0$ covering a range of spectral types namely G7 Ib through K7 Ib. Although Hymphreys (1970) and Hoffleit (1964) assigned a spectral type K5 I to HD216946 thus forcing it on the present list, Wilson's (1976) list of K-line emission stars with pronounced chromospheres indicated

that HD 216946 may actually belong to a somewhat later spectral type namely M0 I. However, this star was even then observed. The list consisted of about 35 stars. Because of unfavourable skies during the monsoon months (from April till July), not all the stars on the list could be observed. In all, we have obtained spectra of 23 stars. Basic data for the program stars are given in Table 1. The first three columns in this table give the HR number, the HD number and the name of the star. The fourth column indicates the spectral type of the star obtained from Wilson (1976) for the stars studied by him and for the rest of the stars from the Catalogue of Bright Stars (Hoffleit 1964). Visual magnitudes and the (B-V) colours are given in the fith and sixth columns respectively. These were taken from Humphreys (1970). In the seventh column $M_{V's}$ are listed. 14 out of the 23 stars have chromospheric CaII H and K emission. For 12 of them, the absolute magnitudes are taken from Wilson (1976) obtained from his study of CaII H and K chromospheric emission. They are marked with asterisks. $M_{V's}$ for HD 89388 and β Ara are obtained from Warner (1969). M_V for HD 62576 is obtained from Luck (1977).

For studying the outer layers of the atmospheres including the chromospheres and the CS shells, it is

Table 1

Star HR	HD	Name	Spectral type	V	B-V	M_V	M_{bol}
237	4817		K5 Ib	6.07	1.74		
834	17506	η Per	K3 Ib	3.76	1.69	-3.8*	-4.3
861	17958		K3 Ib	6.51			
2473	48329	ϵ Gem	G8 Ib	3.08	1.40	-4.5*	-4.7
2580	50877	O'CMa	K3 Iab	3.78	1.73	-4.7*	-5.2
2615	52005	41 Gem	K3 Ib	5.62	1.66	-3.1*	-3.6
2646	52877	σ CMa	K7 Ib	3.46	1.74	-4.2*	-5.3
2764	56577		K3 Ib	4.83	1.71	-4.1*	-4.6
2993	62576		K3 Ib	4.58	1.63	-4.3*	-4.8
3225	68553		K3 Ib	4.44	1.62		
3612	77912		G7Ib-II	4.60	1.04	-2.2*	-2.4
3634	78647	λ Vel	K5 Ib	2.30	1.70	-3.8*	-4.9
3692	80108		K3 Lb	5.11	1.66		
4050	89388		K5 Ib	3.39	1.54	-3.7	-4.8
4120	91056		K3 Ib	5.26	1.86		
5742	137709		K5 Ib	5.25	1.75		
6461	157244	ζ Ara	K3 Ib	2.84		-4.0	-4.5
7114	174947	33 Agr	K1 Ib	5.75	1.18		
7866	196093	47 Cyg	K2 Ib	4.72	1.61		
8079	200905	ξ Cyg	K5 Ib	3.72	1.66	-2.0*	-3.1
8308	206778	ϵ Peg	K2 Ib	2.42	1.54	-4.1*	-4.5
8465	210745	ζ Cep	K1 Ib	3.35	1.58	-4.7*	-5.0
8726	216946		M0 Ib	4.98	1.80	-4.4*	-5.6

important to know the actual geometrical extent of the stars. The inner radius of the shell and its thickness are two important parameters in determining the physical conditions in the envelope. This radius together with the escape velocity at that radius determine whether mass ejection is taking place and also the rate at which it is taking place if at all. Few direct determinations of radii of these stars exist. A common indirect method is to use the relation $L = 4\pi R^2 \sigma T_{eff}^4$ to obtain R, the radius provided the luminosity L and the effective temperature T_{eff} are already known from other data.

Unfortunately the effective temperatures are available for only 9 program stars while the luminosities are known for 16 of them. Table 2 lists the stars for which the effective temperatures and luminosities are known. These have been adopted from Luck (1977, 1979). Then the absolute bolometric magnitudes were calculated using the bolometric corrections due to Johnson (1966). Because of the intrinsic dispersion of about $0^m.5$ in the absolute magnitudes (Keenan 1978), the radii obtained for these stars are only good to a factor of 2 or so. The radii obtained for the stars ranging in spectral type (G8-K5) are of the order of 10^{13} cm. For the analysis of line profiles, we have

Table 2

Star	Spectral Type	M_V	M_{bol}	Log $(L/L_\odot)$	T_{exc}(°K)	Teff(°K)	Log gSP	Log g_{EV}	$R/R_\odot$	$R_* \times 10^{13}$ (cm)
η Per	K3 Ib	-3.0	-4.3	3.86	3700	4275	1.00	1.00	157	1.1
ϵ Gem	G8 Ib	-4.5	-4.7	3.82	3950	4575	0.85	1.20	129	0.9
α CMa	K3 Iab	-4.7	-5.2	4.02	3500	4150	0.75	0.90	200	1.4
1 Pup	K3 Ib	-4.3	-4.6	3.81	3800	4300	1.30	1.10	143	1.0
ζ Cyg	K5 Ib	-2.0	-3.1	2.97	3575	4075	1.75	1.60	57	0.4
ϵ Peg	K2 Ib	-4.1	-4.5	3.70	3775	4375	1.00	1.20	129	0.9
μ Cep	K1 Ib	-4.7	-5.0	3.94	3800	4400	1.00	1.00	157	1.1
β Ara	K3 Ib	+0.6	-0.4	2.05		4600	1.30	2.50	17	0.1
λ Vel	K5 Ib	-2.8	-3.3	3.21		4250	1.40	1.50	71	0.5

Log g_{gp} and g_{EV} are the spectroscopic and evolutionary gravities respectively.

$L/L_\odot$ is the ratio of the luminosity of the star to that of the Sun.

T_{exc} the excitation temperature - all these parameters are taken from Luck (1977, 1979).

R_* is the radius of the star.

assumed the radius to be 10^{13} cm, for all the stars.

b. Coude spectrograms of λ Vel, η Per and o^{1} CMa were obtained on Kodak 098-02 emulsion using the coudé spectrograph on the 40" telescope. Useful spectra for these stars were mostly obtained in December 1977 and January 1978. The Coude spectrograph is comprised of collimator mirror of 8" aperture, a camera mirror of 16" aperture and a 400ℓ/mm grating blazed at 5000Å in the second order giving a dispersion of 4.2Å/mm in the second order. The reduction factor (collimator focus/ camera focus) was 2 for the coudé spectrograph. The slit width was fixed at 50-60μ such that the projected slit width on the photographic plate was 25-30μ . The resolution on the plate was thus 0.128Å. The stellar spectra were taken in the second order. The Kodak filter OGI was inserted in the beam of light passing through the slit to cut off light from the overlapping orders. The spectral range covered was $\lambda\lambda$6200-6800. The exposure times for obtaining unwidened spectra of these stars varied between 2 and 5 hours depending upon sky conditions. Becuase of such large exposure times, it was not possible to widen the spectrum.

Echellé spectrograms were obtained for all the 23 program stars with the Echellé spectrograph at the coudé focus of the 40" telescope using an uncooled single stage image tube (Varo type) and a 7" camera. The Echellé spectrograph has a 79 ℓ /mm echelle grating blazed at 6746Å in the 34th order where the H_α line lies. The cross dispersion grating used is a 300 ℓ /mm grating blazed at 6400Å. The collimator mirror has an aperture of 6" and a focus of 60". With the camera mirror of 7" focus, the reduction factor becomes 8.5. The dispersion is approximately 10.5Å/mm at and around H_α . The comparison spectrum was of neon. Stellar spectra were obtained for a few stars on 098-02 plates and for the rest on 103a-F films. In all 56 usable spectra have been obtained for the present study, two each of the stars ϵ Gem, ζ Cep, ζ Cyg, ϵ Peg, HD 62576, HD 77912, four for 0^{1}CSa, seven for β Ara and one each of the stars 33 Sgr, HD 4817, HD 80108, HD 89388, HD 91056, HD 196093 and HD 17958. Six spectrograms out of all these were marginally under-exposed. For 10 stars, spectra widened to about .2mm were obtained. For the rest, we had to take recourse to untrailed spectra because of the upper limit on the exposure time with the image tube.

Calibrations for the plates and films were obtained from a quartz prism calibration spectrograph and a rotating sector providing a calibration spectrum in steps of known intensity ratios. The spectra of a few of the stars are shown in Figure 1. Both the plates and films along with the calibrations were traced on the micro-densitometer.

The spectrum ranges from 5800Å to 7800Å. As pointed out by Chaffee and Schroeder (1976), the analysis of an echellé spectrogram differs from the normal procedure. Firstly each order in the echellogram is tilted with respect to the direction of the echelle dispersion. It is a serious handicap if one needs to analyse a large spectral range. The second effect is the variation of the intensity along each order. The density tracings clearly show that the continuum falls quite rapidly towards the two ends of a single order. The analysis of lines present in the falling continuum is possible only if the spectrum corrected for the change in efficiency of the echelle. In order to avoid these complications, we adjusted the echelle grating and the cross disperser such that on each echellogram the H_α line was in the middle of the strip. The continuum in the vicinity of H_α is fairly uniform. The

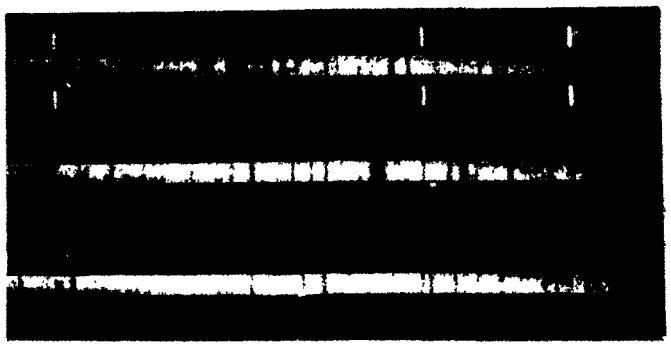

λ Vel K5 Ib

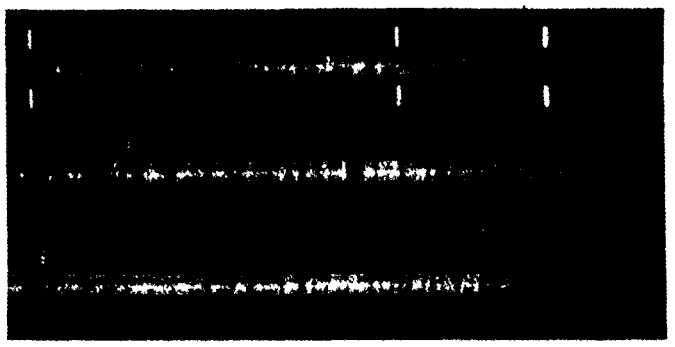

ε Gem G8 Ib

σ CMa K7 Ib

o' CMa K3 Iab

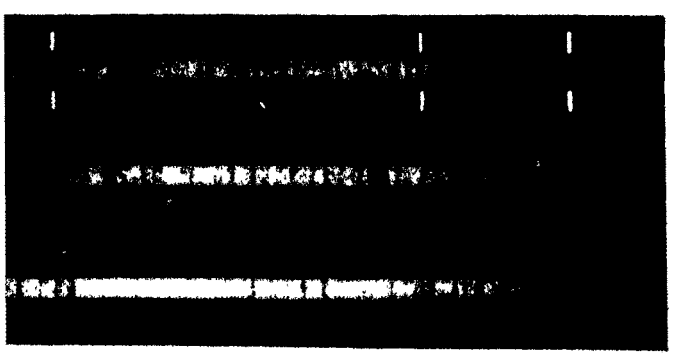

η Per K3 Ib

FIG. 1

H_α profiles of the program stars hardly have any wings, so the line extends over a relatively narrow width. Therefore, the problem of the wings merging into the falling continuum does not arise. The NaI D lines were present three orders away from the H_α towards blue (upwards) where the exposures had already become too faint to show the cores in these lines. Also these lines fall on one edge of the order where further analysis is likely to be dubious. Therefore, the observations once designed for H_α could not be used for analysing the NaI D lines. Similarly the KI $\lambda\lambda$ 7665, 7695 lines were exposed lightly. They were three orders away on the red side of H_α (downwards). Therefore, they were left unexplored too.

The only usable line other than H_α in these spectra is the intercombination line of CaI at λ 6572.781, arising from the transition $(4S^2)^1 S_1 - (4S\ 4P)^3 P_2$. Saite (1973) had observed CaI λ6573 in ζ Aur and had traced its origin to the circumstellar envelope of this well known spectroscopic binary system (K4 Ib + BV Ib). The CaI line is present in the same order as H_α and is rightly exposed. So this line was also studied alongwith H_α to get additional infor- ; around these stars.

c. The Reduction Procedure

The density tracings in the neighbourhood of H_α for a few of the trailed stellar spectra are shown in Figure 2. It is clearly noticeable from these density tracings that the H_α line profiles in all these stars have cores displaced to the blue with respect to the line center. It is hard to place the deepest part of the line on the plate itself because the H_α line is quite broad and the line minimum could easily be mistaken. Instead of measuring the position of the core of the line on the comparator, we determined it on the density tracing itself of each star. The procedure followed is detailed below.

Since the dispersion was found to be non-linear along a single order, independent measurement of positions of a series of comparison lines of thorium present in a single order showed that second degree polynomial fits well the wavelength-distance scale. To determine the scale on the density tracings, we used lines in the stellar spectrum instead of those in the comparison spectrum. Lines were chosen from the same order in which the H_α line appears and not far from H_α which reduces the other adverse effects arising from an echellé spectrum as described earlier.

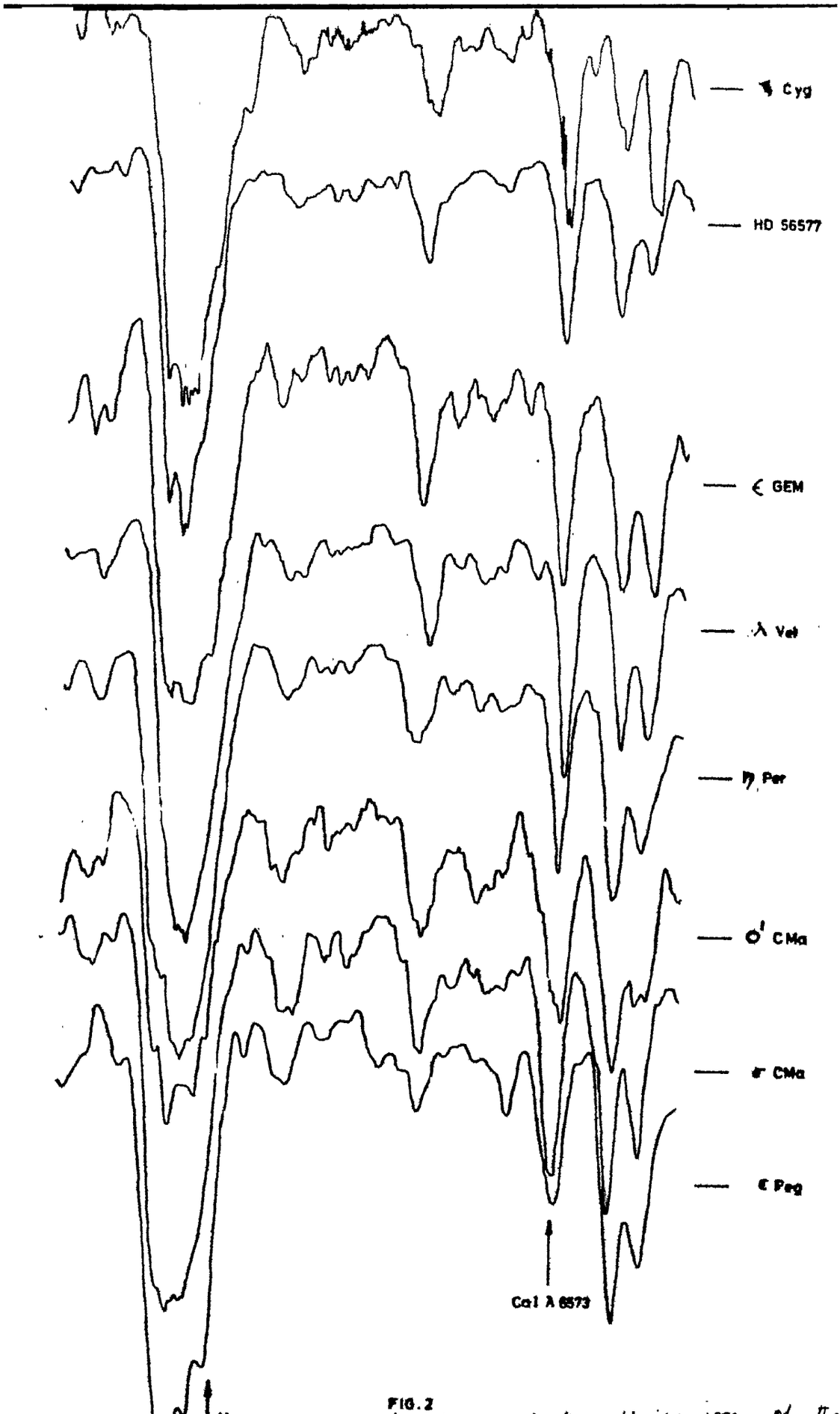

FIG. 2
Density tracings of the Hα region of the spectrum for eight programme stars. Ca I λ 6572 is also indicated.

Lines of high excitation potential were selected because they are most likely of photospheric origin. For each density tracing, the constants of the polynominal satisfying the scale were determined. Using the resultant scale, the position of the core of the $H\alpha$ line was determined using three photospheric FeI lines at $\lambda\lambda$ 6546.248, 6574.238, 6581.220.

It is a common practice in studies of stellar atmospheres to express line core displacements in terms of velocities. These displacements are presumably Doppler in origin in the sense that the absorption core is formed in a column of material moving with respect to the star giving a Doppler shift of the line center in the star's rest frame. In this case the displacements measured in terms of wavelengths can be expressed in units of velocity with the help of the relation

$$\frac{\Delta\lambda}{\lambda_0} = \frac{v}{c}$$

where $\Delta\lambda$ is the wavelength shift from the line center at λ_0 and v is the velocity shift.

In the analysis of theoretical line profiles, these shifts in wavelength/frequency and velocity are more commonly expressed in units of Doppler width and thermal velocity respectively. The thermal velocity is defined by $(2kT/m)^{\frac{1}{2}}$ where T is the excitation

temperature of the line under consideration and m is the mass of the hydrogen atom. If the average excitation temperature for the $H\alpha$ line in the programme stars is assumed to be 4000°K, then one thermal unit is equivalent to 8.13 km/sec. The Doppler width in frequency units is given by $\frac{\nu_0}{c}\left(\frac{2kT}{m}\right)^{1/2}$ and in wavelength units by $\frac{\lambda_0}{c}\left(\frac{2kT}{m}\right)^{1/2}$. For H_α, the unit Doppler width equivalent of wavelength is 0.178Å.

The displacement of the line core can now be expressed in terms of velocity shifts. The velocity shifts obtained for the programme stars vary between 4 and 20 km/sec. i.e. from about half a Doppler width to about 3 Doppler widths. An exceptionally high velocity shift was obtained for HD 68553 (about -35 km/sec). The velocity shifts of all the stars are given in Table 3. For the six stars with underexposed spectra, the displacements are not very accurate. The accuracy of the measurement is about 1 km/sec, as determined from the error involved in measuring the position of the H_α core. The displacements obtained with respect to the three photospheric lines differ by less than 1 km/sec. Hence the internal accuracy of the measurements is ≤ 1 km/sec.

For locating the continuum, use was made of the Arcturus Atlas (Griffins, 1968). α Boo, being a K giants has a spectrum similar to that of the K supergiants in the present study. The spectral regions free of lines in the density tracings of these stars were marked with the help of the corresponding clear regions in the tracing of α Boo where the signal/noise ratio is very high. Then a smooth continuum was drawn by joining these several points.

In 13 out of the 23 stars, weak emission is detected above the level of the continuum, for 10 stars to the blue and for the remaining 3 stars to the red side. Equivalent widths of these small emission components were measured - they range from 0.05Å to 0.15Å. The amount of emission crucially depends upon the chosen level of the continuum. The amount of shift of these emission components to the blue or the red in terms of wavelengths are shown in Table.3. On the density tracings of many of the untrailed spectra, it was difficult to detect the weak emission feature at the edges, for it could be easily mistaken with the noise in the continuum.

In each case the density profile was converted into intensity profile using the calibration spectrum

for that star. These observed line profiles were corrected for instrumental broadening by the method of Burger and Van Cittert as modified by de Jager and Neven (1966), According to this method, the following integral equation is solved by an iterative procedure

$$T_n(\lambda) = T_{n-1}(\lambda) + R(\lambda) - \int_{-\infty}^{\infty} T_{n-1}(x)\, A(\lambda - x)\, dx$$

where $T_n(\lambda)$ is the true profile, $R(\lambda)$ the recorded profile and $A(\lambda)$ is the instrumental or the apparatus profile. For the first iteration $T_1(\lambda) = R(\lambda)$ Then $T_2(\lambda) = 2R(\lambda) - \int_{-\infty}^{\infty} R(x)\, A(\lambda - x)\, dx$. The iteration is carried on until $|T_n(\lambda) - T_{n-1}(\lambda)| \leq \epsilon$ where $\epsilon = .001$.

The instrumental profile was chosen to be that of a very faint neon line obtained from the neon-discharge tube using the same instrumental setup.

A computer program was written to obtain the final profiles corrected for instrumental broadening. Three iterations were enough to give a proper convergence of the corrected profile. The representative corrected profiles of the 23 stars are shown in Figure 3.

Equivalent widths were measured from these normalised intensity profiles of the program stars. The

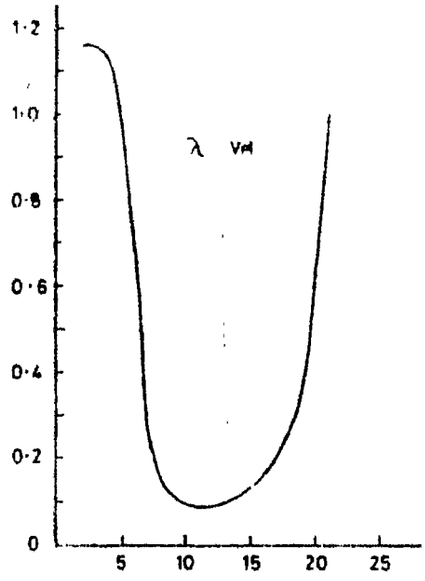

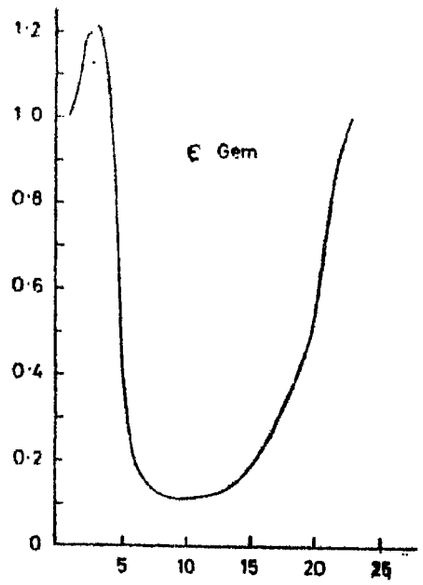

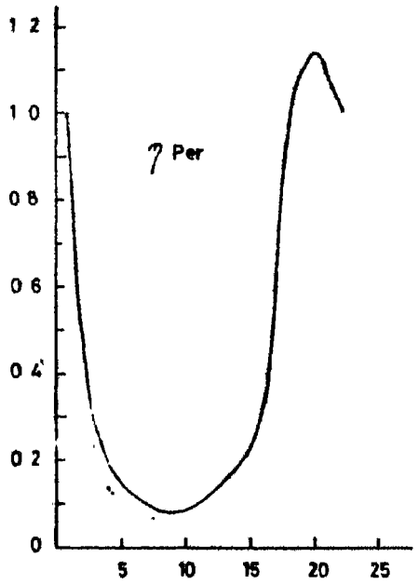

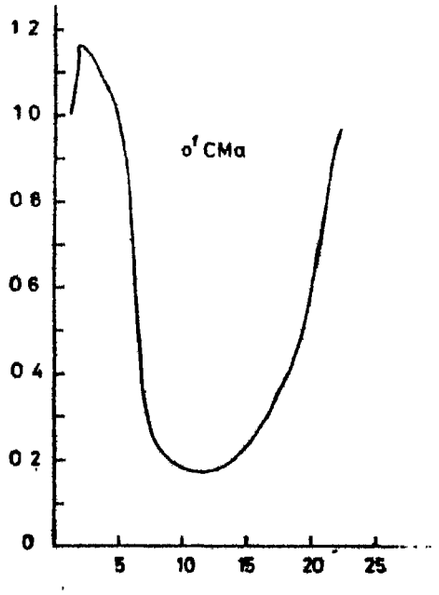

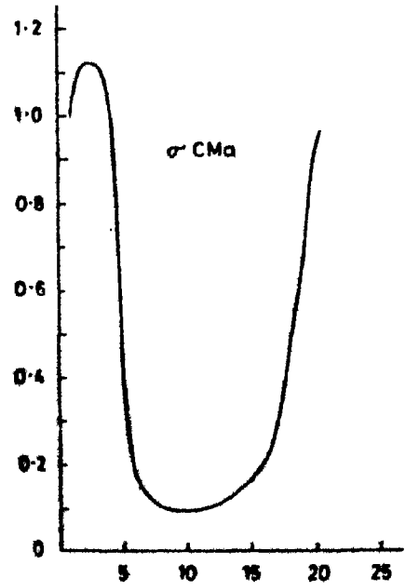

FIG. 3

Corrected Hα profiles of the programme stars

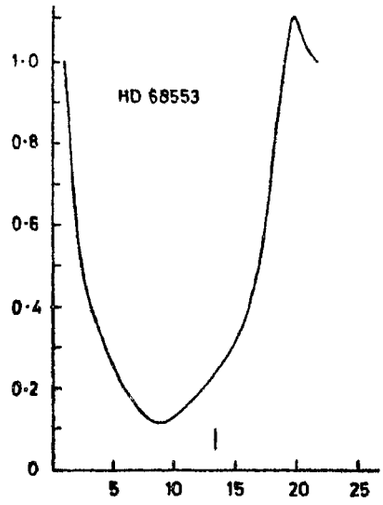
HD 68553
1·0
0·8
0·6
0·4
0·2
0
5
10
15
20
25

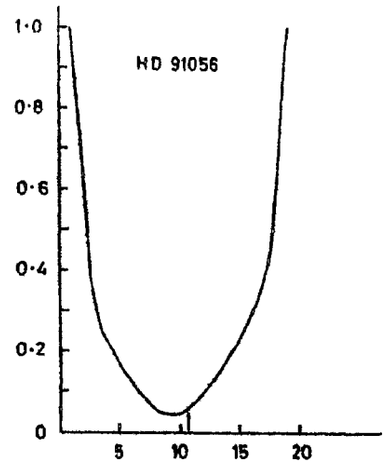
HD 91056
1·0
0·8
0·6
0·4
0·2
0
5
10
15
20

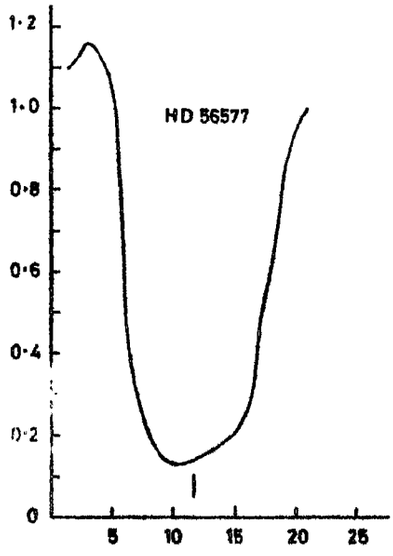
HD 56577
1·2
1·0
0·8
0·6
0·4
0·2
0
5
10
15
20
25

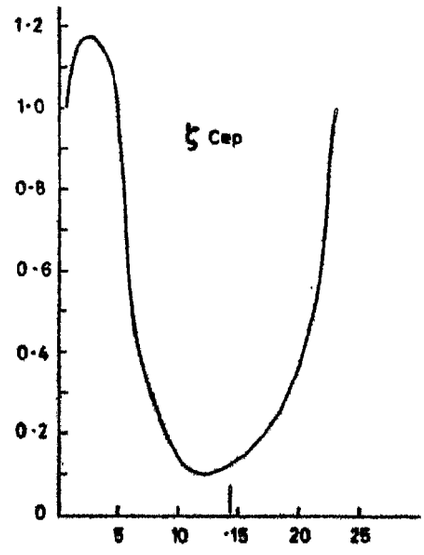
ζ Cep
1·2
1·0
0·8
0·6
0·4
0·2
0
5
10
15
20
25

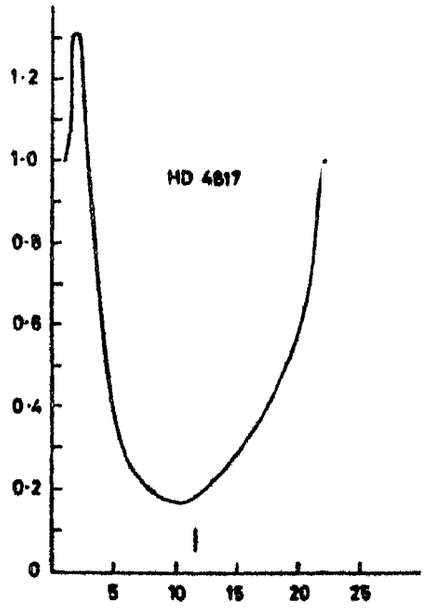
HD 4817
1·2
1·0
0·8
0·6
0·4
0·2
0
5
10
15
20
25

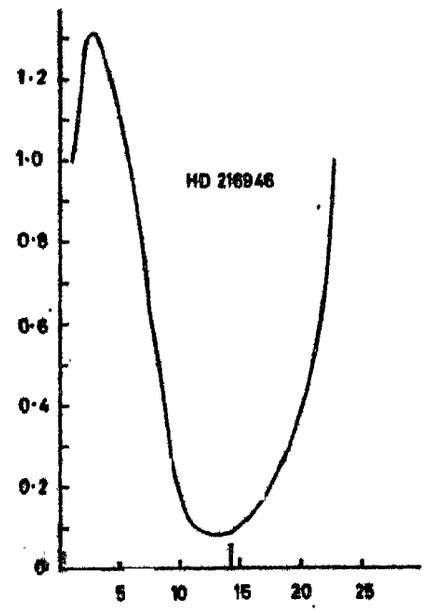
HD 216946
1·2
1·0
0·8
0·6
0·4
0·2
0
5
10
15
20
25

FIG. 3 (Contd)

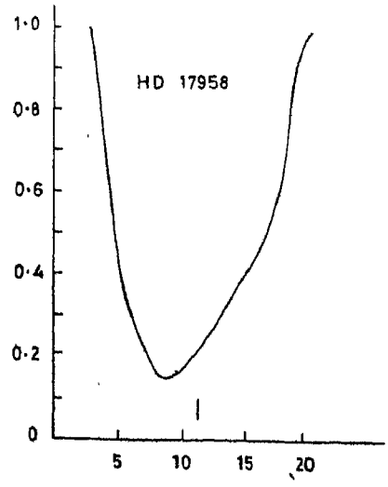
HD 17958
1·0
0·8
0·6
0·4
0·2
0
5
10
15
20

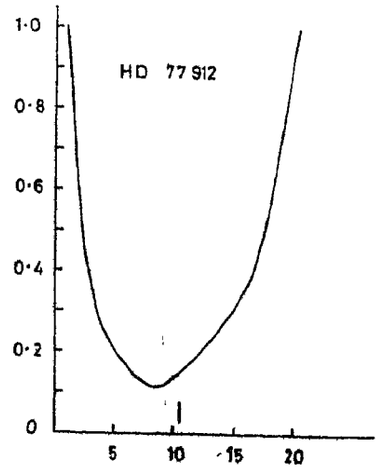
HD 77912
1·0
0·8
0·6
0·4
0·2
0
5
10
15
20

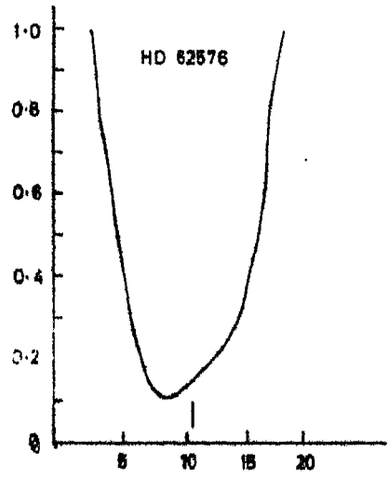
HD 62576
1·0
0·8
0·6
0·4
0·2
0
5
10
15
20

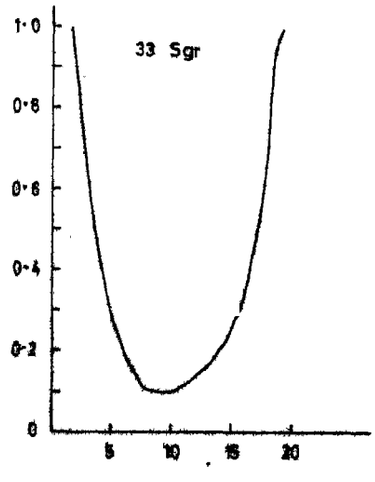
33 Sgr
1·0
0·8
0·6
0·4
0·2
0
5
10
15
20

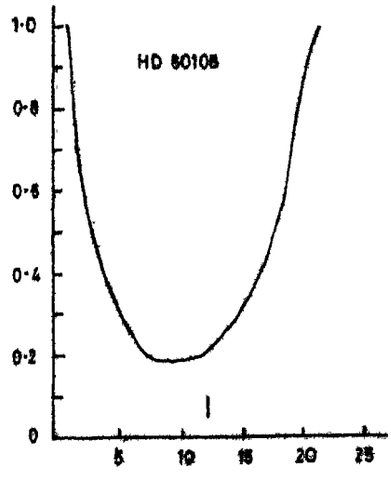
HD 80108
1·0
0·8
0·6
0·4
0·2
0
5
10
15
20
25

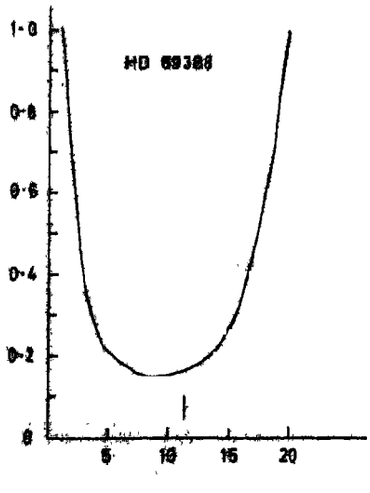
HD 89388
1·0
0·8
0·6
0·4
0·2
0
5
10
15
20

FIG. 3 (Contd)

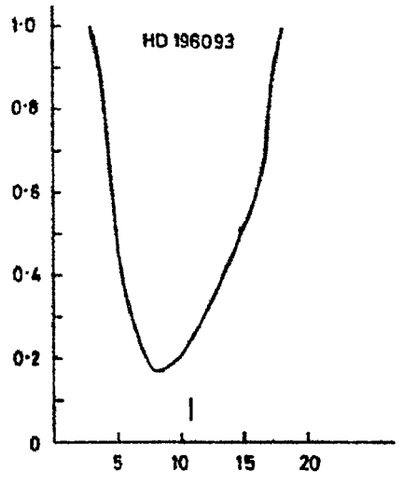
HD 196093
1·0
0·8
0·6
0·4
0·2
0
5
10
15
20

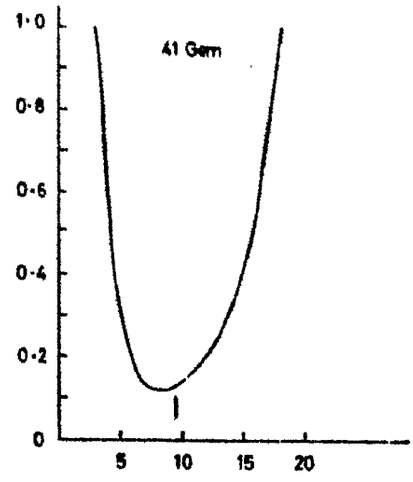
41 Gem
1·0
0·8
0·6
0·4
0·2
0
5
10
15
20

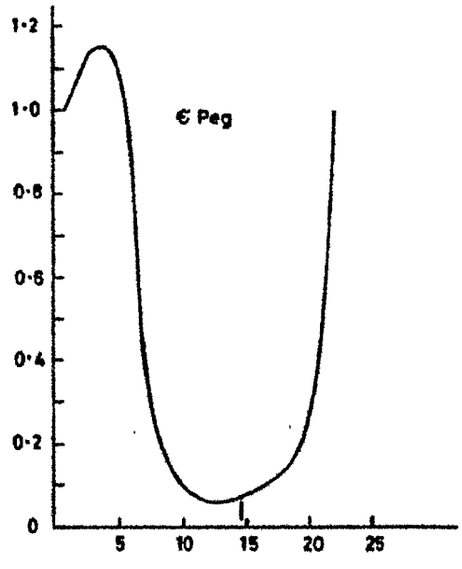
€ Peg
1·2
1·0
0·8
0·6
0·4
0·2
0
5
10
15
20
25

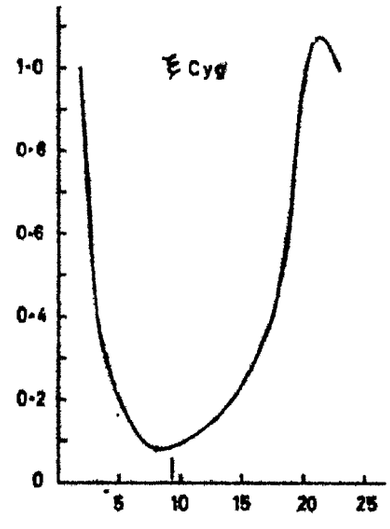
ε Cyg
1·0
0·8
0·6
0·4
0·2
0
5
10
15
20
25

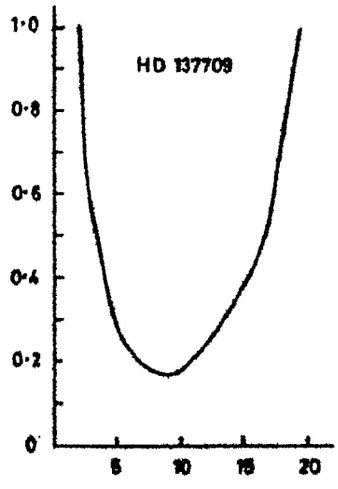
HD 137709
1·0
0·8
0·6
0·4
0·2
0
5
10
15
20

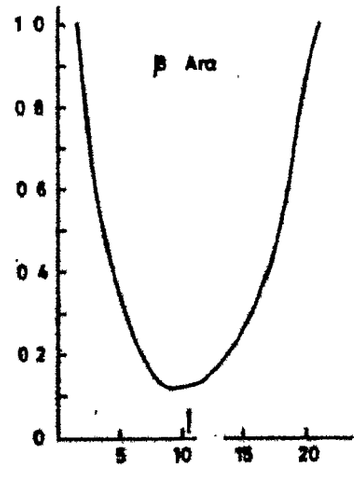
β Ara
1 0
0 8
0 6
0 4
0 2
0
5
10
15
20

FIG. 3 (Contd)

equivalent widths determined from various plates and/or films of the same star agree quite well. The equivalent widths of these H_α absorption profiles along with those of the H_α emission components are listed in Table 3. Equivalent widths as well as the velocity shifts of the CaI] λ 6573 were also measured. These velocity shifts are much smaller than the H_α velocity shifts. Both the equivalent widths and the velocity shifts are listed for CaI in Table 3. Table 4 gives the H_α velocity shifts and the equivalent widths for the three stars λ Vel, O'CMa and η Per observed at the coudé spectrograph.

d. Correlations

For a preliminary analysis, correlations were sought between the various quantities determined observationally. A plot made between the equivalent widths and the velocity shifts of the H_α absorption is displayed in Figure 4. The scatter is too large to show any definite relation between the two. A plot was also made between the ratio of the width of H_α line in the continuum to its depth and the velocity shifts of the absorption core of H_α and is shown in Figure 5. This plot indicates the nature of the velocity field of the line forming region. Although the scatter is

Table-3

Star	No.of plates/ films	Spectral Type	Shift of the H_α line core (km/sec.)	EQW of H_α absorption (Å)	EQW of H_α emission (Å)	Shift of the emission from the line center (Å)	EQW of CaI (Å)	Shift of the CaI line core (km/sec.)
HD 77912	2	G7 Ib	-13.4	1.89			.19	-1.3
ϵ Gem	2	G8 Ib	- 8.1	2.07	.09	-1.44	.37	-6.2
33 Sgr	1	K1 Ib	-4.9	1.99			.31	
ζ Cep	2	K1 Ib	-13.8	2.07	.12	-1.78	.51	-6.7
HD 196093	1	K2 Ib	-18.6	1.56				-9.4
ϵ Peg	2	K2 Ib	- 8.7	2.08	.11	-1.99	.41	-3.6
η Per	3	K3 Ib	- 7.5	2.12	.09	+1.86	.32	-2.2
HD 17958	1	K3 Ib	-17.2	1.59			.21	
θ'CMa	3	K3 Iab	- 6.9	1.65	.07	-1.84	.33	-2.0
41 Gem	3	K3 Ib	- 9.2	1.75			.27	
HD 56577	4	K3 Ib	- 6.1	1.66	.09	-1.46	.44	-1.1
HD 62576	2	K3 Ib	-15.4	1.58			.26	-0.1
HD 68553	3	K3 Ib	-30.1	1.89	.04	+1.57	.27	-10.9
HD 80108	1	K3 Ib	-21.4	1.92	.09	+2.15	.36	-11.6
HD 91056	1	K3 Ib	- 8.7	2.15			.62	-2.2
β Ara	7	K3 Ib	-18.3	1.97			.39	-11.8
HD 4817	1	K5 Ib	-12.0	2.07	.05	-1.70	.43	- 8.8
λ Vel	3	K5 Ib	-11.8	2.04	.13	-1.57	.34	- 0.8
HD 89388	1	K5 Ib	-22.9	2.08			.27	-2.0
HD 137709	3	K5 Ib	- 9.3	1.98			.37	-4.4
ξ Cyg	2	K5 Ib	- 9.3	2.32	.05	+2.08	.49	- 4.1
σ CMa	3	K7 Iab	-10.6	1.93	.09	-1.60	.44	- 1.7
HD 216946	2	M0 Ib	-17.1	2.12	.15	-2.19	.37	- 6.0

Table 4

Star	Spectral type	Shift of the H_α line core (km/sec)	EQW of H_α absorption (Å)
η Per	K3 Ib	-5.1	1.76
α CMa	K3 Iab	-7.2	1.35
λ Vel	K5 Ib	-10.2	1.72

Notes: The H_α equivalent widths measured from the Coudé spectrograms are systematically lower than the ones obtained from the Echellograms. This is because the former are not corrected for instrumental broadening.

a bit too large, there is a definite trend in the sense that for increasing core displacements the ratio becomes smaller. No clear dependence of the equivalent widths or the velocity shifts upon the spectral type were found (see Figure 6 and Figure 7). A plot was made between the H_α and the CaI] velocity shifts. There is a linear correlation between the two (Figure 8). Another plot between the CaI] equivalent widths and H_α velocity shifts is displayed in Figure 9. These two quantities also seem to be linearly related. The significance of all the above correlations will be discussed in a later Chapter.

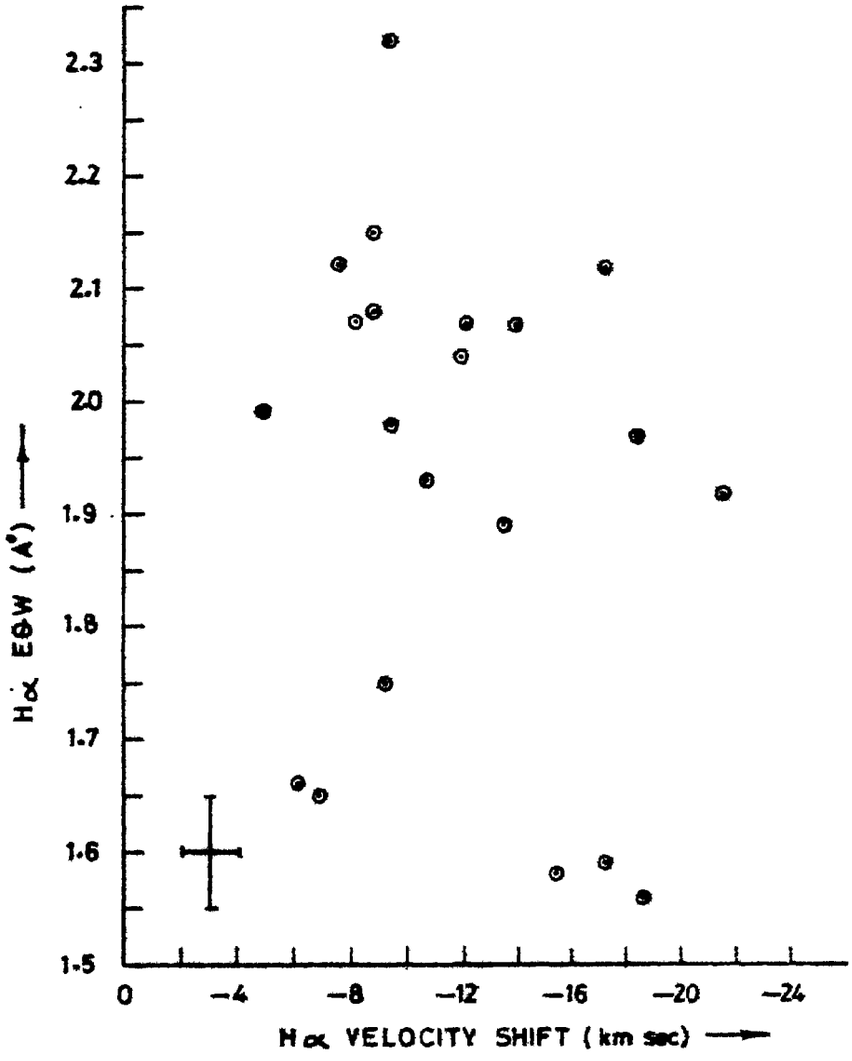

FIG. 4

Equivalent width vs. Velocity shifts of Hα Absorption

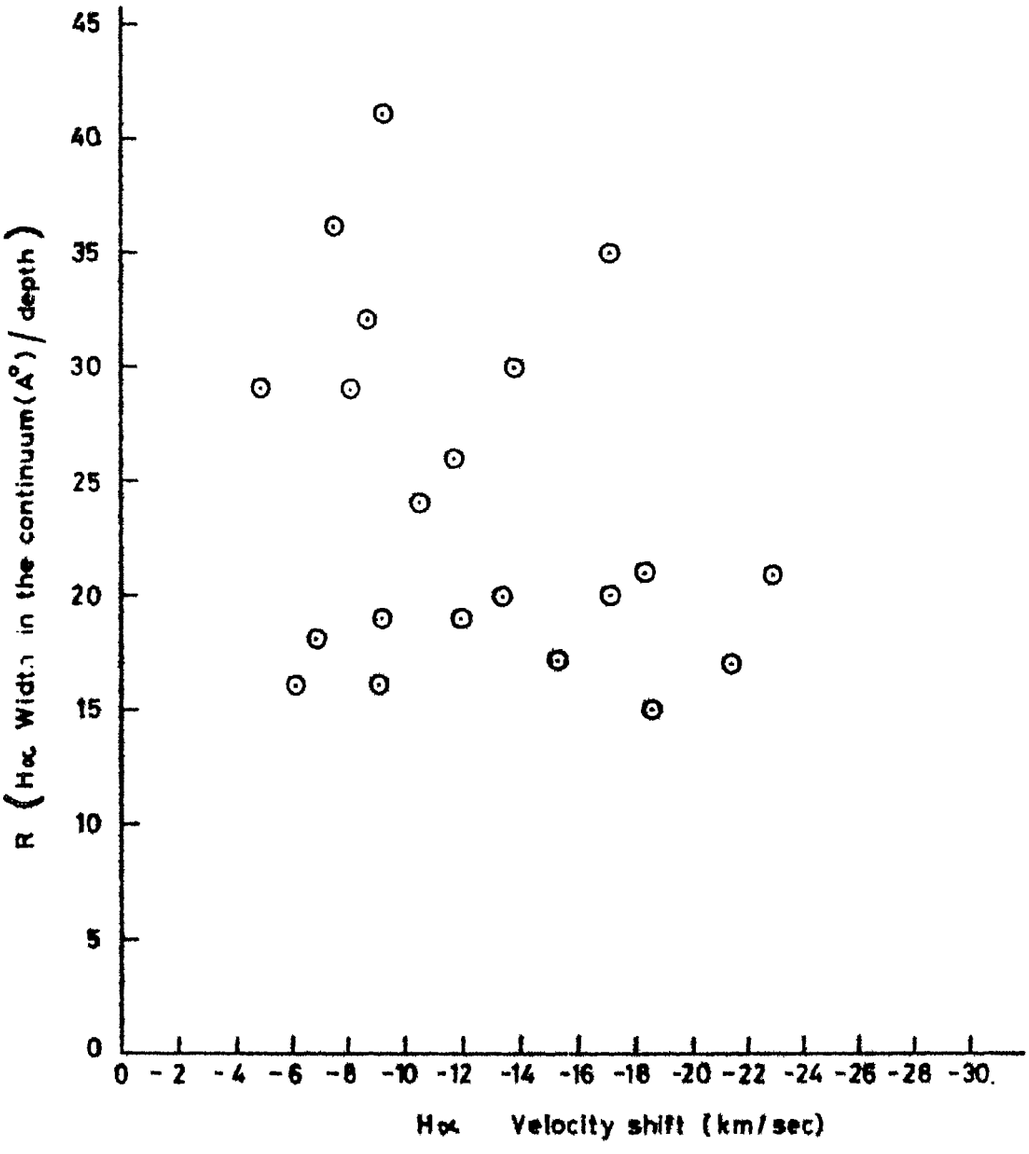

FIG. 5

Width / Depth Vs. Velocity Shift of Hα Absorption

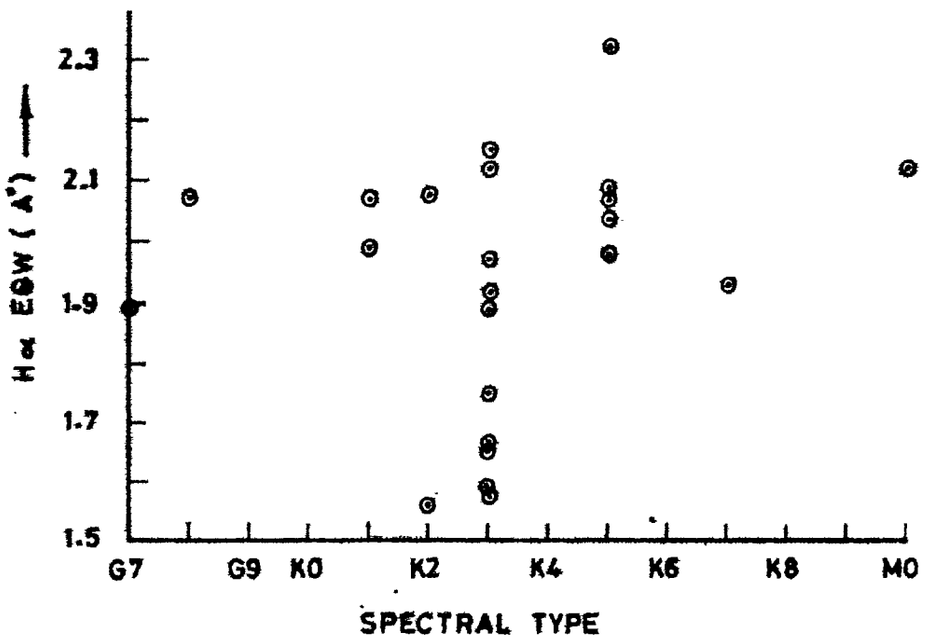

FIG. 6

Equivalent width of Hα vs. spectral type

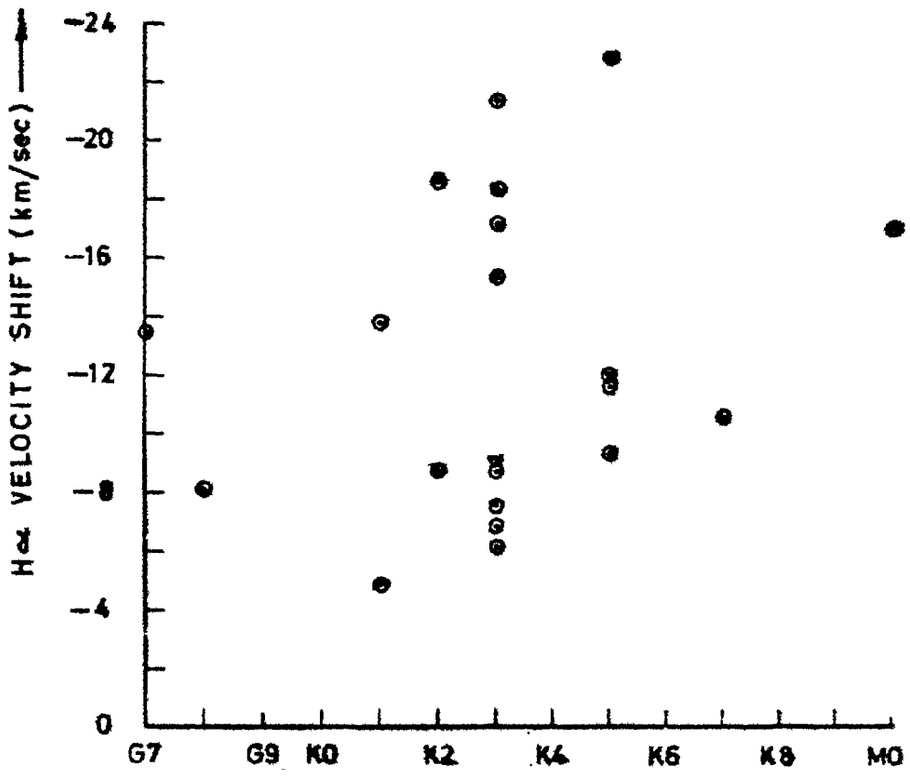

FIG. 7

Velocity Shift of the Hα core vs spectral type

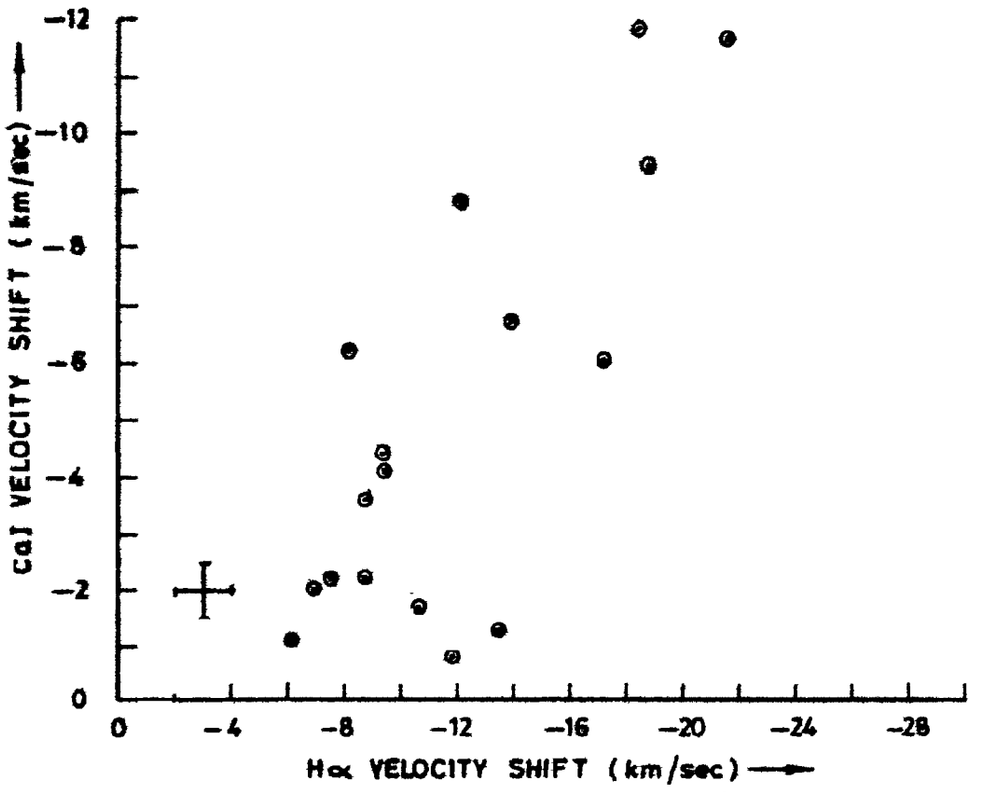

FIG. 8

H_α line core displacement vs CaI] line core displacement

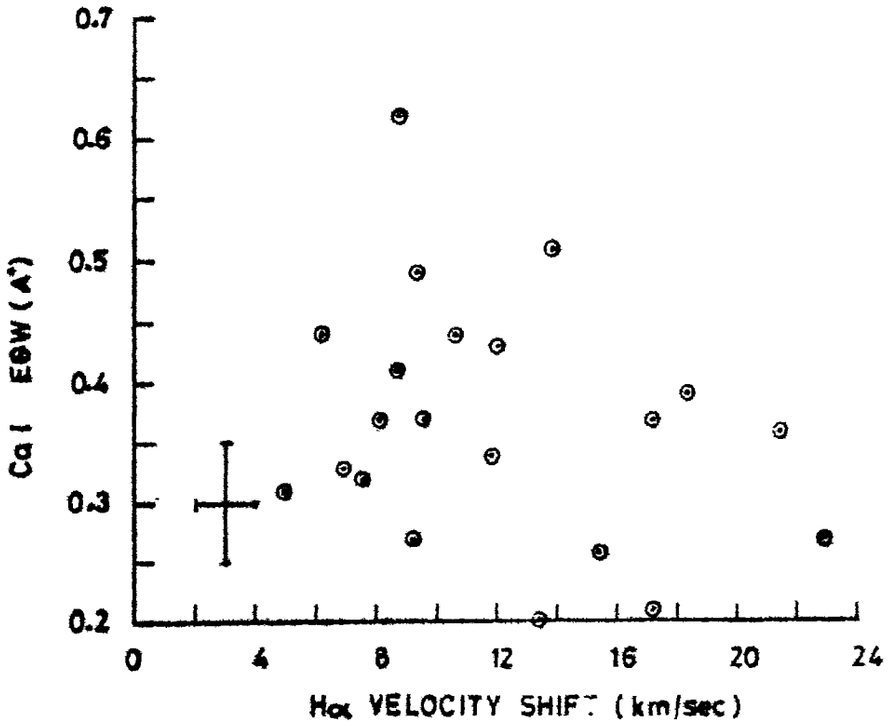

FIG. 9

CaI] Equivalent width vs Hα velocity shifts

CHAPTER III

THEORETICAL COMPUTATION OF THE H_α LINE

To extract from the observed H_α line information pertaining to the physical conditions in the line forming region of the atmosphere, we need to compute theoretical line profiles by using a proper formulation of the radiative transfer problem and vary the input parameters such as optical depth, turbulent velocity and expansion velocity in this problem to reproduce the observed features of the line in question in the absence of a consistent model. The best fit to the observed profile then determines the physical properties of the particular line forming region.

Since supergiant atmospheres are extended, the assumption of a plane-parallel geometry to describe the radiative transfer in these atmospheres is not proper. A spherically symmetric formulation of the transfer problem is the first requirement to obtain meaningful insights into the physical situation. Moreover, since the observed line profiles are all asymmetric in the sense that the absorption cores are displaced to the blue with respect to the line centre in the observer's frame, there is a strong indication of some kind of motion, most likely a net outward motion in these

atmospheres. To interpret the profiles, therefore, one needs to extend the theoretical treatment further to include velocity fields. The basic theory of radiative transfer in spherically symmetric expanding atmospheres has been developed over the last decades and discussed extensively by various authors in a number of astrophysical contexts. The theory is outlined in some detail in the text by Mihalas (1978).

Since we are concerned with line formation and as the line forming region for H_α may extend from the photosphere to the very outer layers of the atmosphere where the medium is tenuous and the radiation field weak, significant departures from LTE are expected to occur. Hence a non-LTE approach is needed. To obtain a self-consistent solution to the line-transfer problem, one should solve the equation of radiative transfer and the equation of statistical equilibrium simultaneously.

According to Athay and Thomas (1958) bulk of the absorption in the H_α line in stars like the sun arises in the lower chromospheres. Weymann (1962) also has suggested that the H_α line in α Ori originates in an enormously extended chromosphere surrounding the star. The lower chromospheres of these stars have large optical depths in the Lyman lines. The implies

a detailed balance in the Lyman-line transitions. The $H\alpha$ line then behaves in a fashion similar to resonance lines. As in the case of resonance lines, the statistical equilibrium equation for a two level atom (levels 2 and 3) is thus adequate for the study of H_α .

For the level n = 2 this may be written as

$$n_2\left(B_{23}\int \varphi_\nu J_\nu d\nu + C_{23}\right) = n_3\left(A_{32} + B_{32}\int \varphi_\nu J_\nu d\nu + C_{32}\right) \quad \text{.. (3.1)}$$

where B_{23} and B_{32} and A_{32} are the Einstein A and B coefficients for the transition $2 \rightarrow 3$ in H. The first term on the right hand side denotes radiative absorptions per unit volume per sec and the second, collisional excitations per unit volume per sec. On the left hand side, the first two terms define the spontaneous and the induced emissions per unit volume per sec respectively. The 3rd term gives the collisional deexcitations per unit volume per sec.

The equation of radiative transfer in a moving atmosphere can be formulated either in the star's rest frame known as the observer's frame or in the comoving frame. In the first case, the observer is at rest and

views the stellar material flowing out while in the second case the transfer problem is treated in a frame in motion with the matter. The comoving frame formulation is particularly suited to handle large scale velocity fields and rapid atmospheric expansion wile the observer's frame method is only restricted to velocities of a few Doppler widths. Since the velocities involved in the present problem are of the order of a few Doppler widths, one could choose either the observer's frame or the comoving frame.

The equation of radiative transfer for a spherically symmetric expanding atmosphere and its solution are adopted from the work of Peraiah (1979). Although designed to treat the line transfer in rapidly moving atmospheres, this formulation is equally valid for the low velocity regime we are interested in.

According to Peraiah (1979) the equation in the comoving frame is given by

$$\mu \frac{\partial I(x,\mu,\tau)}{\partial \tau} + \frac{1-\mu^2}{\tau} \frac{\partial I}{\partial \mu}(x,\mu,\tau)$$

$$= \chi_l \left[\beta + \phi(x,\mu,\tau)\right] \left[S(x,\mu,\tau) - I(x,\mu,\tau)\right]$$

$$+ \left[(1-\mu^2)\frac{V(\tau)}{\tau} + \mu^2 \frac{dV(\tau)}{d\tau}\right] \frac{\partial I(x,\mu,\tau)}{\partial x} \quad \text{.. (3.2)}$$

and for the oppositely directed beam,

$$-\mu \frac{\partial I(x,-\mu,\tau)}{\partial \tau} - \frac{1-\mu^2}{\tau} \frac{\partial I(x,-\mu,\tau)}{\partial \mu}$$
$$= \chi_l \left[\beta + \phi(x,-\mu,\tau)\right]\left[S(x,-\mu,\tau) - I(x,-\mu,\tau)\right]$$
$$+ \left[(1-\mu^2)\frac{V(\tau)}{\tau} + \mu^2 \frac{dV(\tau)}{d\tau}\right] \frac{\partial I(x,-\mu,\tau)}{\partial x}$$

.. (3.3)

Here $I(x,\mu,\tau)$ is the specific intensity at an angle $\cos^{-1}\mu$ at a radial point τ in the atmosphere and frequency $x = (\nu-\nu_0)/\Delta\nu_D$ where $\Delta\nu_D$ is the Doppler width. The total source function $S(x,\pm\mu,\tau)$ is defined as the ratio of emissivity to opacity and is given by Peraiah (1978).

$$S(x,\pm\mu,\tau) = \frac{\phi(x,\pm\mu,\tau)\,S_l(x,\pm\mu,\tau) + \beta\,S_c(\tau)}{\phi(x,\pm\mu,\tau) + \beta}$$

... (3.4)

where S_l denotes the line source function and S_c that in the continuum.

The line source function is expressed in detail as

$$S_l(x,\pm\mu,\tau) = \frac{1-\epsilon}{\phi(x,\pm\mu,\tau)} \int_{-\infty}^{\infty} dx' \int_{-1}^{+1} R(x,\pm\mu;\, x',\mu')\, I(x',\mu')\, d\mu' + \epsilon B(\tau), \qquad \text{.. (3.5)}$$

$$\epsilon = \epsilon' / (1+\epsilon')$$

$$\epsilon' = C_{32}\left(1 - e^{-h\nu/kT}\right) / A_{32} \qquad \text{.. (3.6)}$$

ϵ' represents photons that are destroyed by collisional deexcitation following a photoexcitation, ρ is α_c/χ_l the ratio of opacity in the continuum to that in the line $\phi(x,\pm\mu,\tau)$ and $R(x,\pm\mu;\, x',\mu')$ are the profile and redistribution functions respectively. V (r) defines the velocity field in the moving atmosphere

In the solution of equations (3.2) - (3.5) Peraiah (1979) assumed the following:

a) the profile function ϕ was taken to correspond to the pure Doppler case given by

$$\phi(x, \pm\mu V) = \frac{1}{\delta\sqrt{\pi}} e^{-(x \pm \mu V)^2 / \delta^2} \quad \text{.. (3.7)}$$

where the frequency $x \rightarrow x \pm \mu V$ in the rest frame of the observer and $V = V_{gas}/V_{thermal}$ the ratio of the gas velocity to the thermal velocity; δ was put equal to one,

b) the redistribution function $R(x, \pm\mu; x', \mu')$ was angle-averaged in 4 directions and is given by R_{I-A} (Hummer 1962, Peraiah 1978)

c) $\epsilon = 0$ and $\beta = 0$; the case of a scattering medium, and

d) the outer velocity in the atmosphere was taken to be 10 thermal units.

The line source function $S_L(\tau)$ at the radial points obtained from the solution is shown in Figure 10.

For the study of the H_α line, the above theoretical analysis seems adequate for the following reasons:

(i) the H_α line in late G and K supergiants is well represented by a pure Doppler profile (Kraft et al 1964),

(ii) for a Doppler profile where the width is not very large, the assumption of complete redistribution of photons over the line profile is quite valid,

(iii)Since the H_α line forms in the lower chromospheres of these stars where the optical depth in the continuum is very low while the opacity in the line center of H_α is very large, the ratio $\chi_c/\chi_\ell \sim 0$

(iv) Since the excitation of the H_α line requires more than 10eV of energy and the local kinetic temperatures in the line forming regions of these stars are low, collisions are not effective in forming the line; at the same time the photoionization edge of the level $n = 2$ falls in a region of the spectrum where the stellar radiation field is rather strong. Hence the line belongs to the category of photoionization dominated lines (Thomas, 1957, 1965) and appropriately the source function has $\epsilon \simeq 0$,

(v) Although normally the source function is a function of V (r), in an extended atmosphere with a chromospheric temperature rise, it is only weakly affected by the velocity field (Groth and Wellman, 1970) Therefore, the source function displayed in Figure 10 is deemed adequate even for the smaller velocities encountered in the present problem.

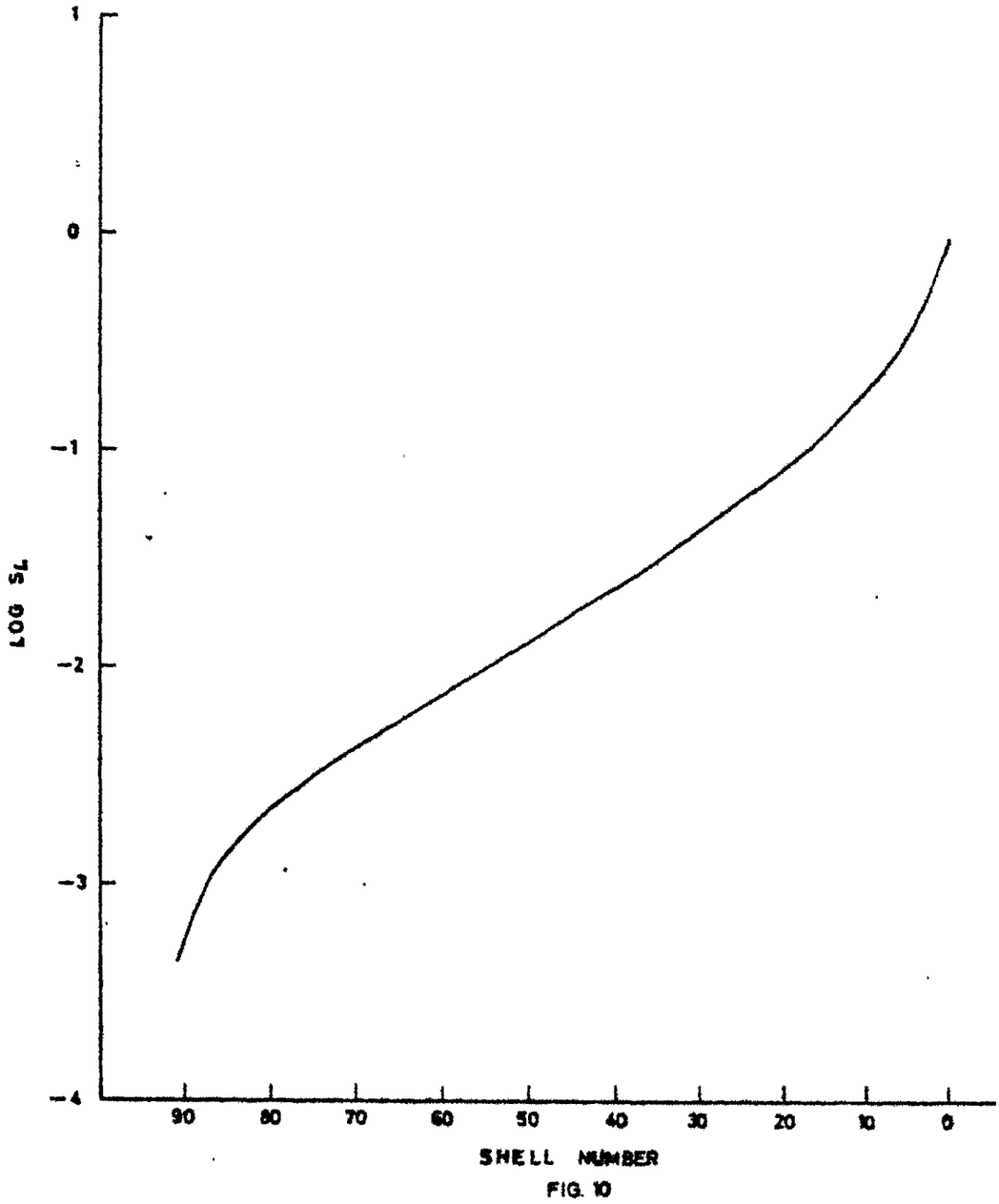

FIG. 10

Plot of the line source function

The observational work on expanding atmospheres (Sanner 1976, Bernat 1977, Hagen 1978 and Boesgaard and Hagen 1979) have so far been only confined to the circumstellar envelopes. In these studies the photospheric contribution to the line profile has always been assumed to be symmetric and subtracted from the composite line profiles. Only the shell contribution to the line has been analysed. The problem of line formation is too complicated to warrant such a separation of the shell profile from the photospheric profile. This is especially true for the H_α line since the CS contribution to the absorption in the line is only a fraction of the total. In the present work, therefore, a continuous distribution of matter is assumed to exist from the photosphere to a maximum extent of 2-3 times the stellar radius.

Using the line source function displayed in Figure 10 in conjunction with appropriate density and velocity distributions (to be described later), the flux in the H_α line as a function of frequency has been computed with the help of a subroutine to the main transfer code also provided by Dr. Peraiah. To do this the following geometry was assumed for the H_α forming regions.

We assume that there is a reasonably well defined photosphere of radius R_{in} surrounded by a spherically symmetric, radially expanding envelope with an outer radius R_{out}. The extent of the envelope is, therefore, $\Delta R = R_{out} - R_{in}$, (see Figure 11). The envelope is divided into a number of shells. Since the velocity distribution V (r), the density distribution $\rho(r)$ and the source function $S_\ell(r)$ obtained after solving equations (3.2) and (3.3), are specified at each sub-shell, the computation of the line flux follows in a fairly straight-forward manner.

The flux F_ν is calculated in the line of sight of the observer at each frequency. The material behind the star is hidden from the observer (occulted region in Figure 11) and that in front gives rise to the absorption.

As the observer views the emission lobes on either side of the star the various radial directions contribute differently to the line-of-sight emission depending upon the $\cos\theta$ factor involved. The intensities are calculated at equally spaced radial points in the line-of-sight and integrated over the thickness of the envelope to yield the total flux in the emission lobes. If I (h) denotes the line-of-sight intensity, the flux

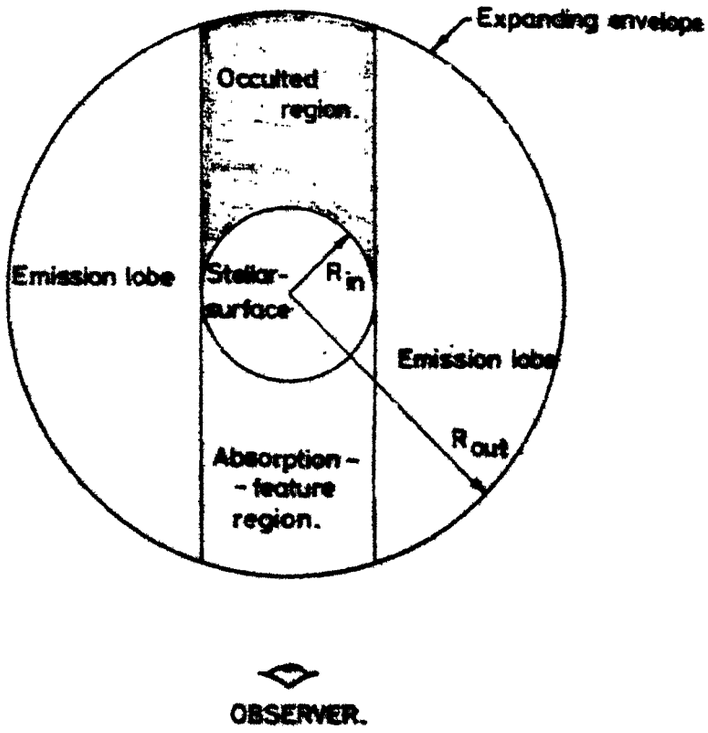

FIG. 11

Geometry of the model envelope

from each emission lobe is given by

$$F_\nu = 2\pi \int_{R_{in}}^{R_{out}} I(h)\, h\, dh$$

The total flux at each frequency then is $f_\nu = F_\nu' + 2 F_\nu$ the factor 2 arising due to the 2 emission lobes.

The results of the line profile computations and the appropriate fits to the observed H_α line profiles are discussed in the next Chapter.

CHAPTER IV

a) Characteristics of the Observed Profiles

The principal characteristics of the H_α line in the G and K supergiants observed are the following:

(i) The line is in deep absorption and reaches a level of (0.05-0.15) of the continuum. The width of the line at the continuum is roughly 3Å.

(ii) There is a distinct shift of the absorption core to the blue giving rise to an asymmetric appearance. This shift in terms of velocity is in the range of -4 to -24 km/sec.

(iii) The equivalent widths are in the range of 1.5-2.3Å. The line is unsaturated and has almost a core-like quality as is seen on all microphotometer tracings.

(iv) Weak emission components are present on the red edge for 4 stars and on the blue edge for 9 stars. The strength of the emission is in the range of 0.05-0.15Å. Emission within the velocity range of the absorption profile is of marginal detectability.

b) H_α - forming regions

The observed H_α line in G and K supergiants is

much too strong for the prevailing physical conditions in these atmospheres. The level n = 2 of hydrogen has to be over/populated by a significant amount with respect to the LTE value to produce the observed strength of the line. Moreover the asymmetry of the line most certainly indicates a net expansion of the layers where this line is formed. Although the problem of formation of this line has not been solved in detail, its observed characteristics are highly suggestive of a chromospheric origin. The asymmetry of the line in that case implies that the chromospheres around these stars are expanding.

c) Analysis of line profiles.

For a complete analysis, one needs to know both the characteristics of the underlying stellar continuum, as also the physical properties of the envelope where the line is formed. In other words, one would have to assume a model of the chromosphere for these stars where the bulk of the H_α absorption occurs.

Given the properties of a star and its appropriate chromospheric model, the problem of H_α -line transfer needs to be solved to generate the theoretical H_α profiles. If such profiles were obtained, a detailed point to point matching of these with the observed

profiles would lead to further improvement in the knowledge of the chromosphere and a vindication of the chromospheric model assumed. Due to the lack of data relating to the chromospheres of these stars, it is not possible to do such an analysis very satisfactorily for each individual star. Also this would involve a prohibitive amount of computing. Moreover, the quality of observations does not warrant such an approach. However, the properties of the envelope can still be determined by comparison of the gross chracteristics of the observed and theoretically computed profiles. For example, the equivalent width of the line is a measure of the total absorption and a function of the column density of the line forming atoms. The displacement of the absorption core indicates the departure from the static nature of the atmosphere. The width at the continuum and the half-width of the line are both dependent upon the turbulence and the velocity structure in the atmosphere. Based on the analysis given in the previous Chapter and the geometry described in Figure 11, theoretical profiles have been generated and compared with the observed to determine column densities and velocity fields in the outer atmospheres of the program stars.

(1)

The equivalent width (EQW) is a measure of the strength of the line and is defined by

$$W_\lambda = \int_{\lambda_0-\Delta\lambda}^{\lambda_0+\Delta\lambda} \left(1 - \frac{F_\lambda}{F_c}\right) d\lambda \qquad \text{.. (4.1)}$$

where F_λ is the flux in the line at a wavelength λ. F_c the flux in the continuum, λ_c the wavelength at the line center and $2\Delta\lambda$ the width of the line in the continuum.

The optical depth at the center of the H_α line is given by

$$\tau_0 = \frac{\sqrt{\pi}e^2}{mc} f N \frac{1}{\Delta\nu_D} \qquad \text{.. (4.2)}$$

$$= \alpha N \qquad \text{.. (4.3)}$$

where N is the column density of the line forming atoms, f the oscillator strength and $\Delta\nu_D$ the Doppler width. In an atmosphere with a density gradient, the number density of hydrogen in level n = 2 (n_2) depends upon the total density at any point as also upon the physical conditions that control the level population. The latter

is determined by the equation of statistical equilibrium. The column density

$$N = \int_{R_{in}}^{R_{out}} n_2 \, dr = \int_{R_{in}}^{R_{out}} \beta n \, dr \qquad .. (4.4)$$

where n is the total number density of hydrogen and β denotes the fraction in n = 2. β involves a Boltzmann factory and a departure coefficient. In the absence of a consistent model of the chromospheric region, the variation of β with depth could not be incorporated. To simulate an over-population in n = 2 with respect to its LTE value a temperature slightly higher than T_{exc} was used instead of the LTE Boltzman factory. The factor β was then absorbed in the constant α of equation (4.3). The f-value for the H_α line was taken from Wiese, Smith and Glennon (1966). It is equal to 0.6407. The Doppler width defined in Chapter II included only the thermal term. In real stellar atmospheres the widths of the metal lines cannot be explained solely on the basis of thermal motion and microturbulence is normally invoked (Mihalas 1978).

If ξ_t denotes the root mean square turbulence, then the expression for the Doppler width is modified as

$$\Delta\nu_D = \frac{\nu_0}{c}\left(\frac{2kT_{exc}}{m} + \xi_t^2\right)^{1/2} \qquad \text{.. (4.5)}$$

According to Kuhi (1973), ξ_t may be as large as 20 km/sec in supergiant atmospheres. The high value may partly be due to the exclusion of non-LTE effects in model atmosphere analysis and partly due to the presence of velocity gradients in these atmospheres. Since the width of the line in the continuum and hence the equivalent width are dependent upon the value of ξ_t, ξ_t was used as a free parameter in the line profile computations. Table 5 gives $\Delta\nu_D$ and a for various values of ξ_t for a given excitation temperature. The velocity parameter

$$V_t = \left(\frac{2kT_{exc}}{m} + \xi_t^2\right)^{1/2} \qquad \text{.. (4.6)}$$

corresponds to a T_{kin} defined by

$$\frac{2kT_{kin}}{m} = \frac{2kT_{exc}}{m} + \xi_t^2 \qquad \text{.. (4.7)}$$

T_{kin} is also given in Table 5.

Table - 5

$T_{exc} = 4000^{\circ}K$

ξ_t (km sec^{-1})	V (km sec^{-1})	T_{kin} ($^{\circ}K$)	$\Delta\nu_D$ (10^{10} sec^{-1})	α	$\Delta\lambda_D$ (Å)
0	8.13	4000	1.239	1.38(-21)	0.178
5	9.54	5512	1.455	1.17(-21)	0.209
10	12.89	10050	1.965	8.69(-22)	0.282
15	17.06	17610	2.601	6.56(-22)	0.384

ii) Density and Velocity Distribution

A priori the density and velocity distributions in the $H\alpha$ line forming region are not known. Various possible combinations of density and velocity distributions, each set satisfying the equation of continuity, were tried in the hope that we could choose a set which best reproduce the chracteristics of the observed profiles. The four cases studied in detail are :-

A Density $n(r)$ = constant and
Velocity $V(r) \propto 1/r^2$,

B Density $n(r) \propto 1/r^2$ and
Velocity $V(r)$ = constant ,

C Density $n(r) \propto 1/r$ and
Velocity $V(r) \propto 1/r$,

D Density $n(r) \propto 1/r$ and
Velocity $V(r) \propto r$.

The first three cases satisfy the equation of continuity corresponding to spherical flow while the last case is appropriate for a plane-parallel flow. In a highly extended atmosphere, it is only proper to use spherical flow. However, the $H\alpha$ line forming region in the supergiants is mostly confined to the

chromosphere whose thickness is only a fraction of the stellar radius. Therefore, it is not wrong to try solutions for a plane-parallel flow.

In the line flux computation code used here the density and velocity distributions were not written explicitly in terms of the radial coordinate. The discretised coordinate used in the program was the shell number which varied from 1 to 90 over the extent of the envelope. In terms of this coordinate, therefore, a linear decrease in density amounts to a total variation of almost two orders of magnitude between the inner and the outer radius. The velocity distribution also given in terms of the discretised coordinate was always consistent and satisfied the equation of continuity. In the chromospheres where the density drop is very rapid the representation in terms of the discretised coordinate seems to be rather convenient.

Each computer run of a set of theoretical profiles is characterised by a density n_H and a velocity at the innver radius V_a, a turbulent velocity ξ_t and the extension of the envelope ΔR. Each profile in the set is characterised by a particular value of the velocity V_b at the outer radius.

In the absence of a velocity gradient (Case B) the inner and outer velocities have the same value and the atmosphere strictly expands with a constant velocity. When a velocity gradient is present, such a clear definition of the velocity of expansion is not obtained. Since the velocity is only a function of the radial co-ordinate r, an average expansion velocity may still be defined as

$$V_{exp} = \frac{\int V(r)\,dr}{\int dr} \qquad \text{.. (4.8)}$$

Some representative line profiles for the various cases are shown in Figure 12. The computed line profiles are seen to have the following characteristics -

1. The EQW increases with the optical depth at the line center.
2. The width of the line in the continuum and, therefore, the EQW increases with increasing velocity gradient.
3. The line core displacement increases linearly with the outer velocity.
4. The turbulence increases the width of the line in the continuum. As a result, the EQW is dependent upon the turbulent velocity.

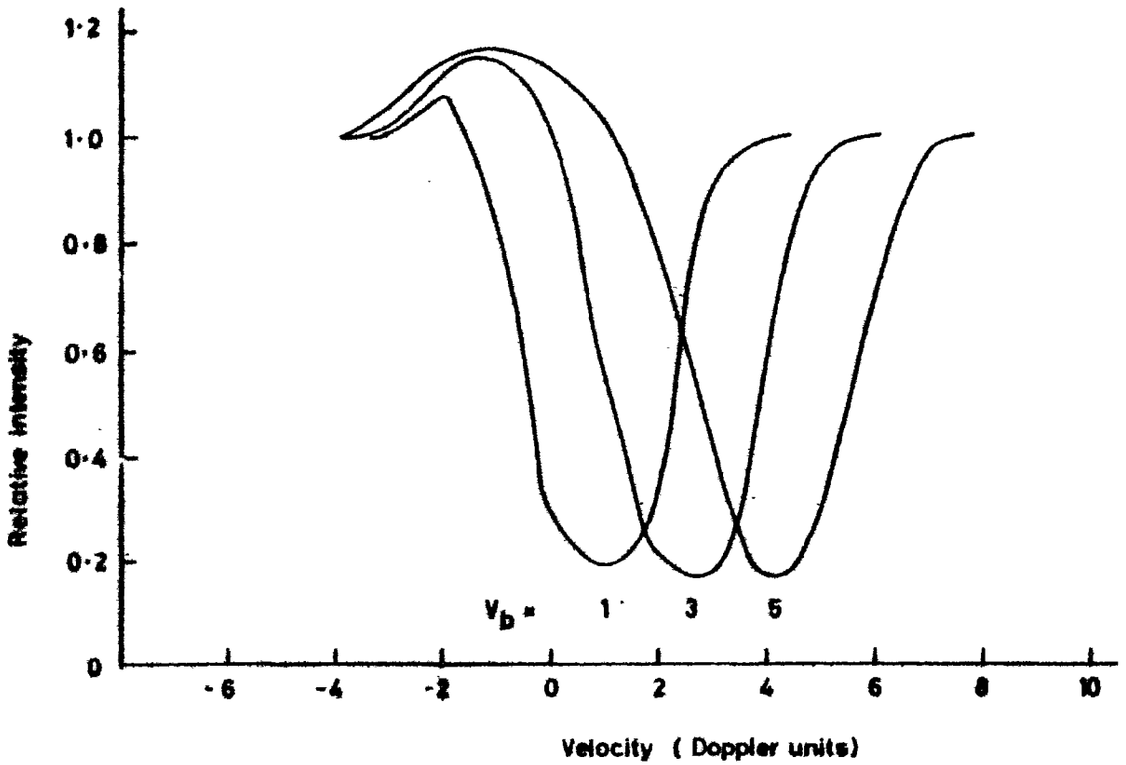

FIG. 12a

Case B computed profiles for $\tau = 62$ and three velocities of expansion V_b labelled in Doppler units.

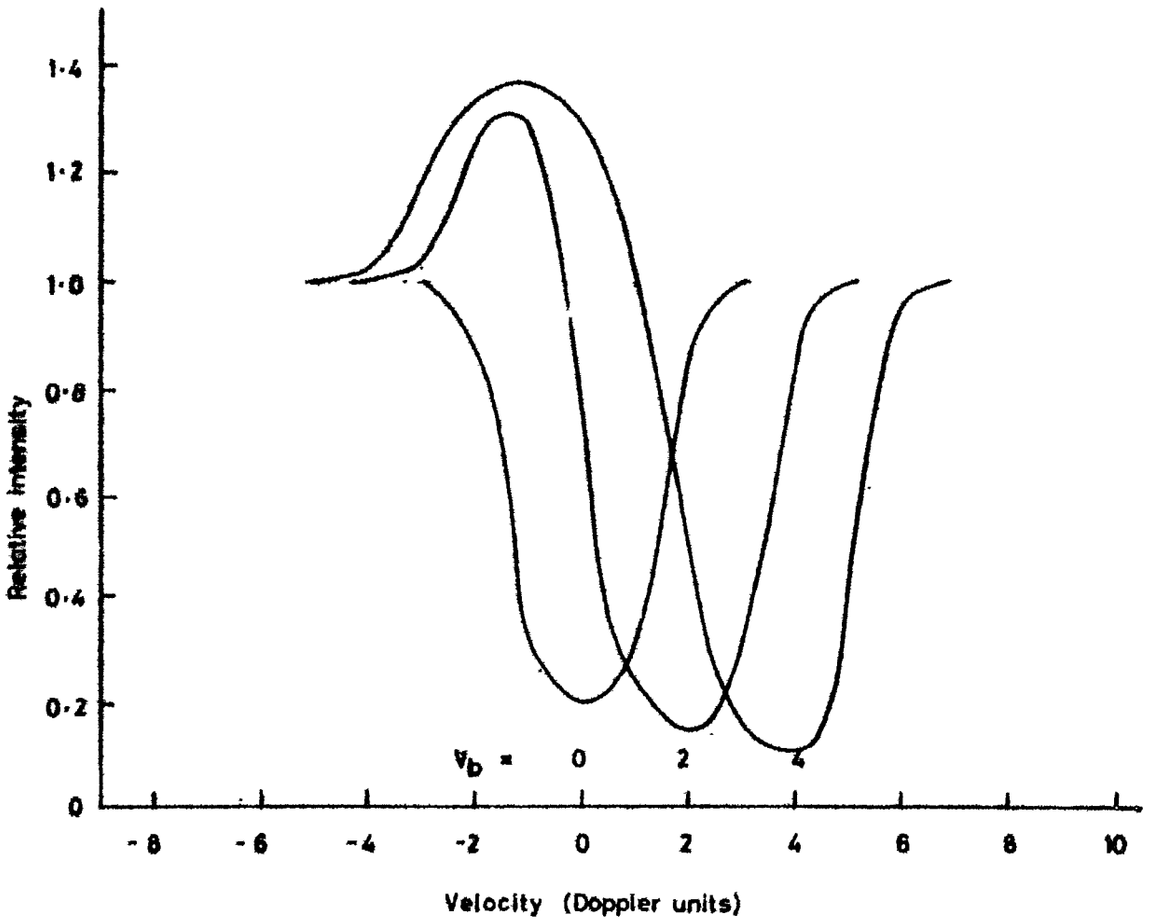

FIG. 12 b

Case B computed profiles for $\tau = 1.24$

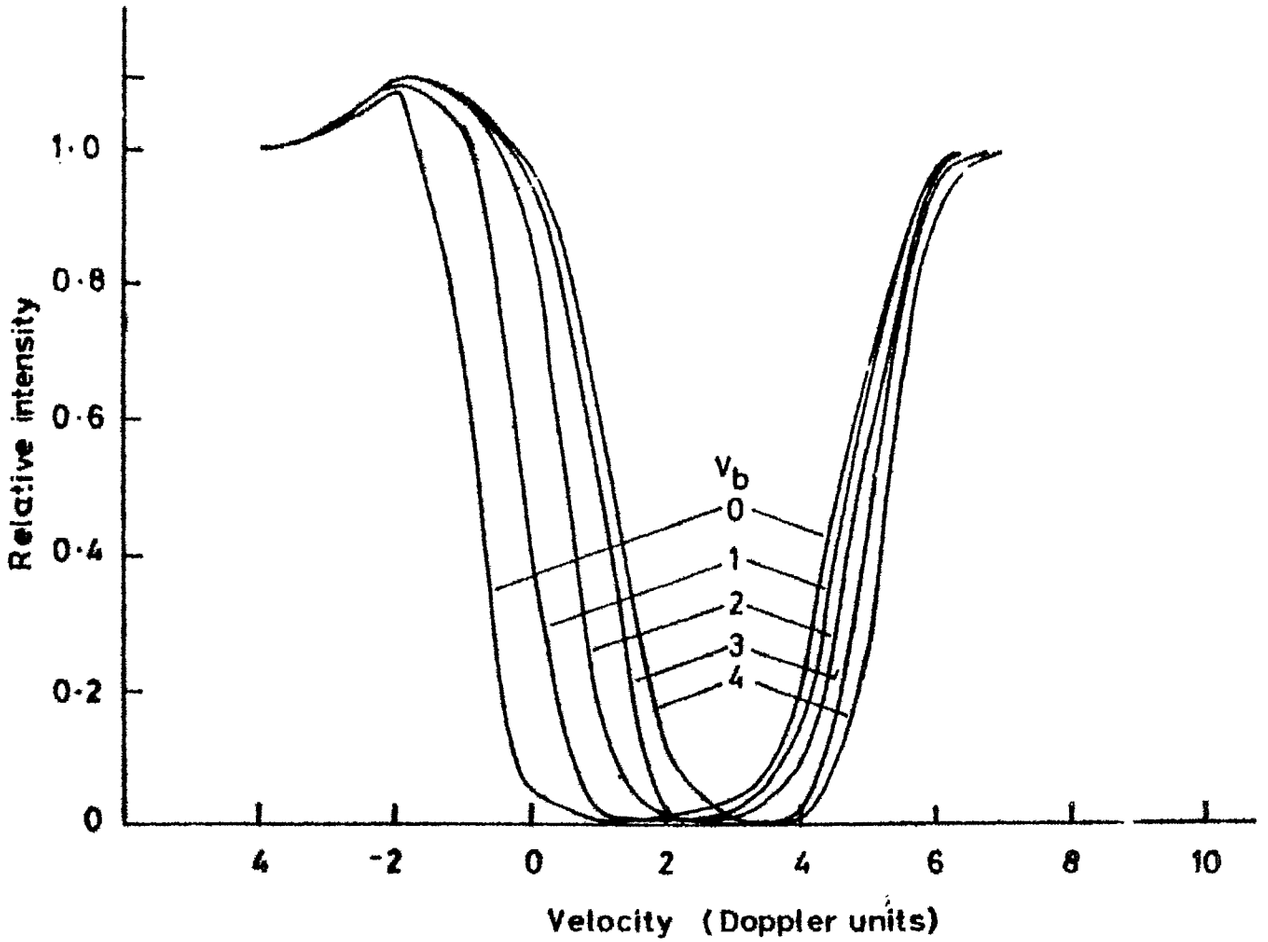

FIG. 12c

Case C computed profiles for $\tau = 47$ and $V_a = 4.0$ Doppler units
Individual profiles are labelled by V_b also in Doppler units

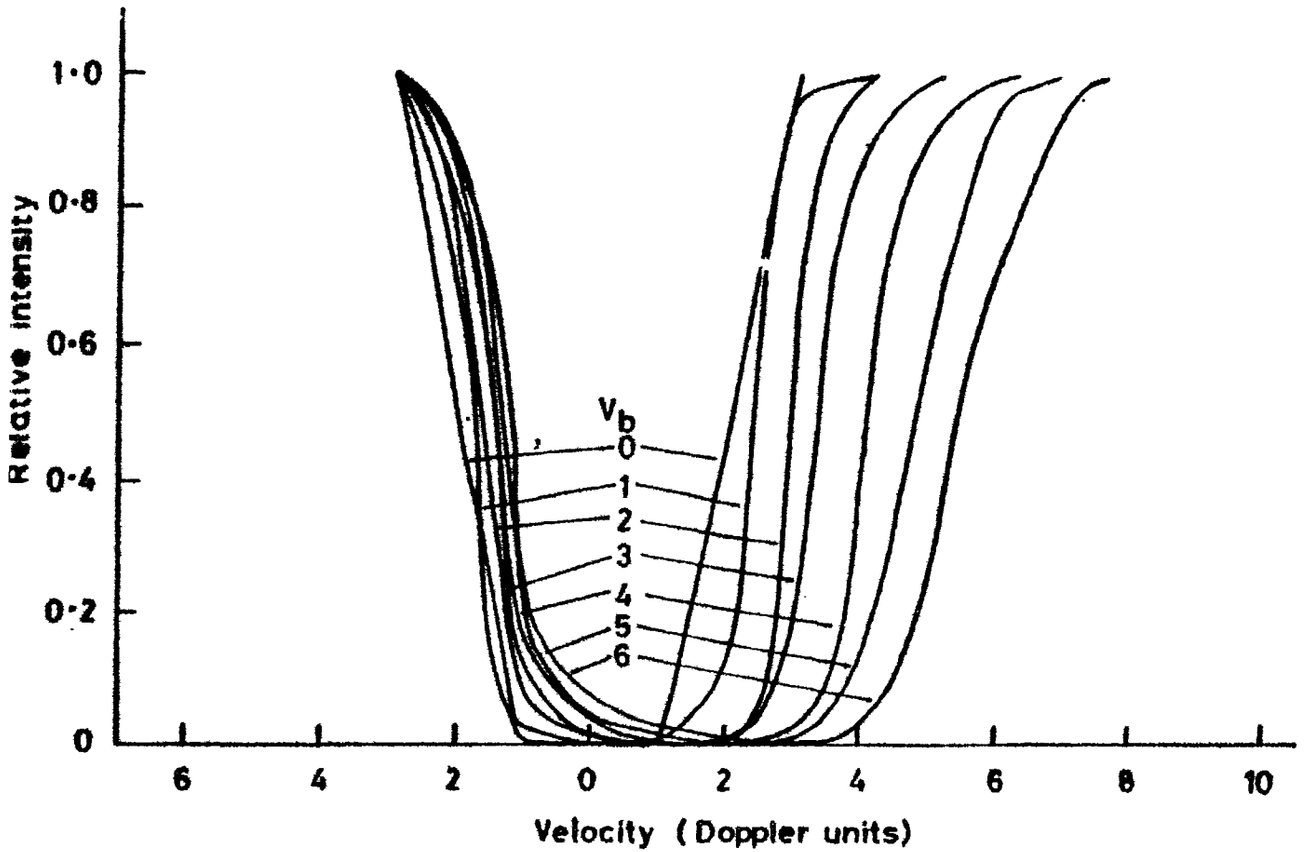

FIG. 12 d

Case D. computed profiles for $\tau = 47$ and $V_a = 0$ The value of V_b in Doppler units for each profile is indicated

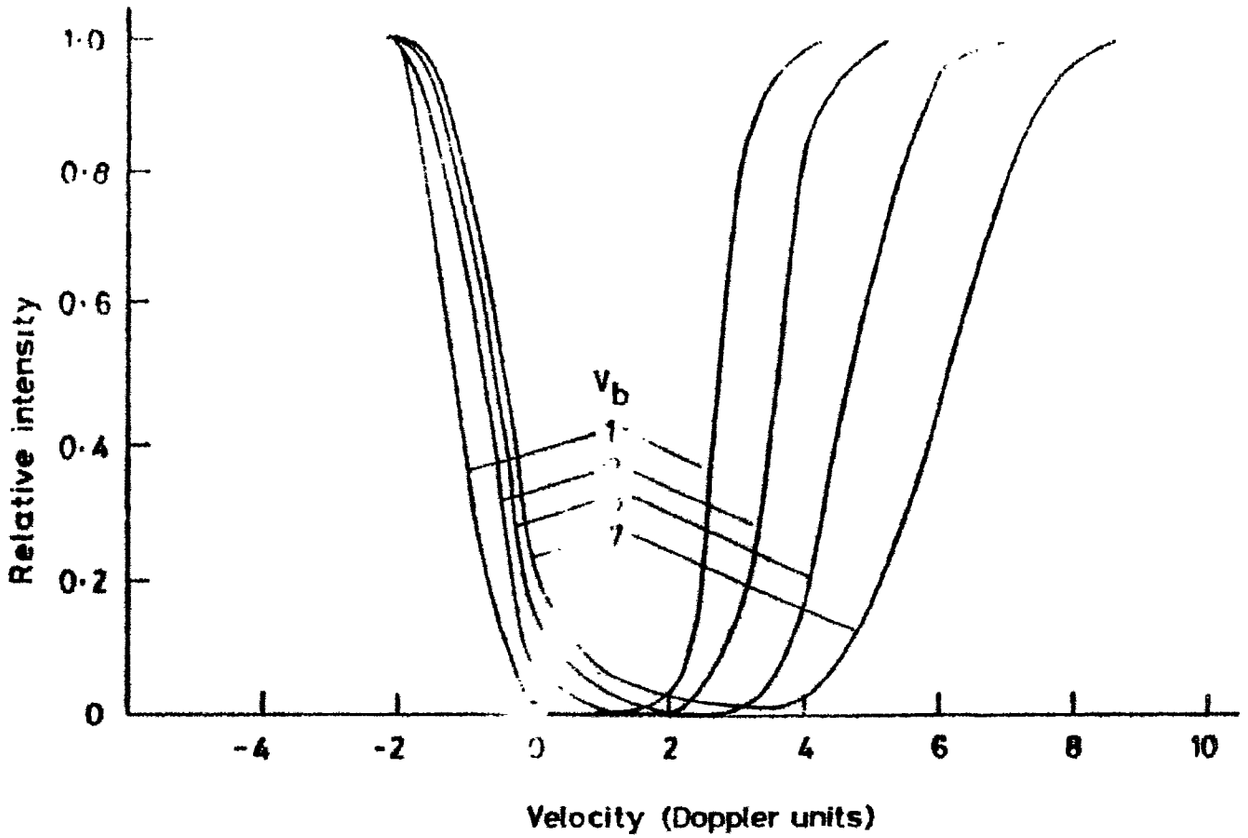

FIG. 13a

Case D computed profiles for $\tau = 31$ and $V_a = 1.0$ Doppler unit.
Each profile is marked by V_b also in Doppler unit.

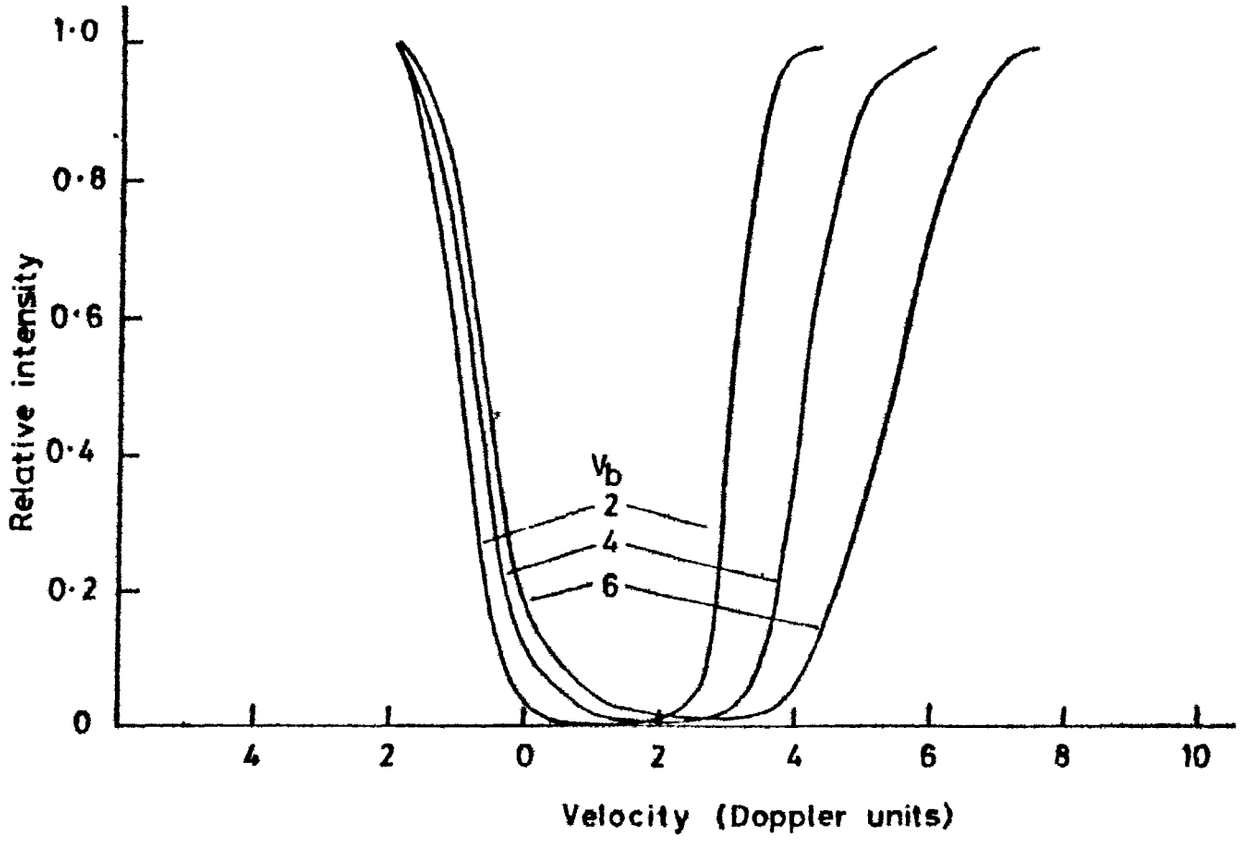

FIG. 13 b

Case D computed profiles for $\tau = 31$ and $V_a = 1.0$ Doppler unit. Each profile is marked by V_b also in Doppler unit.

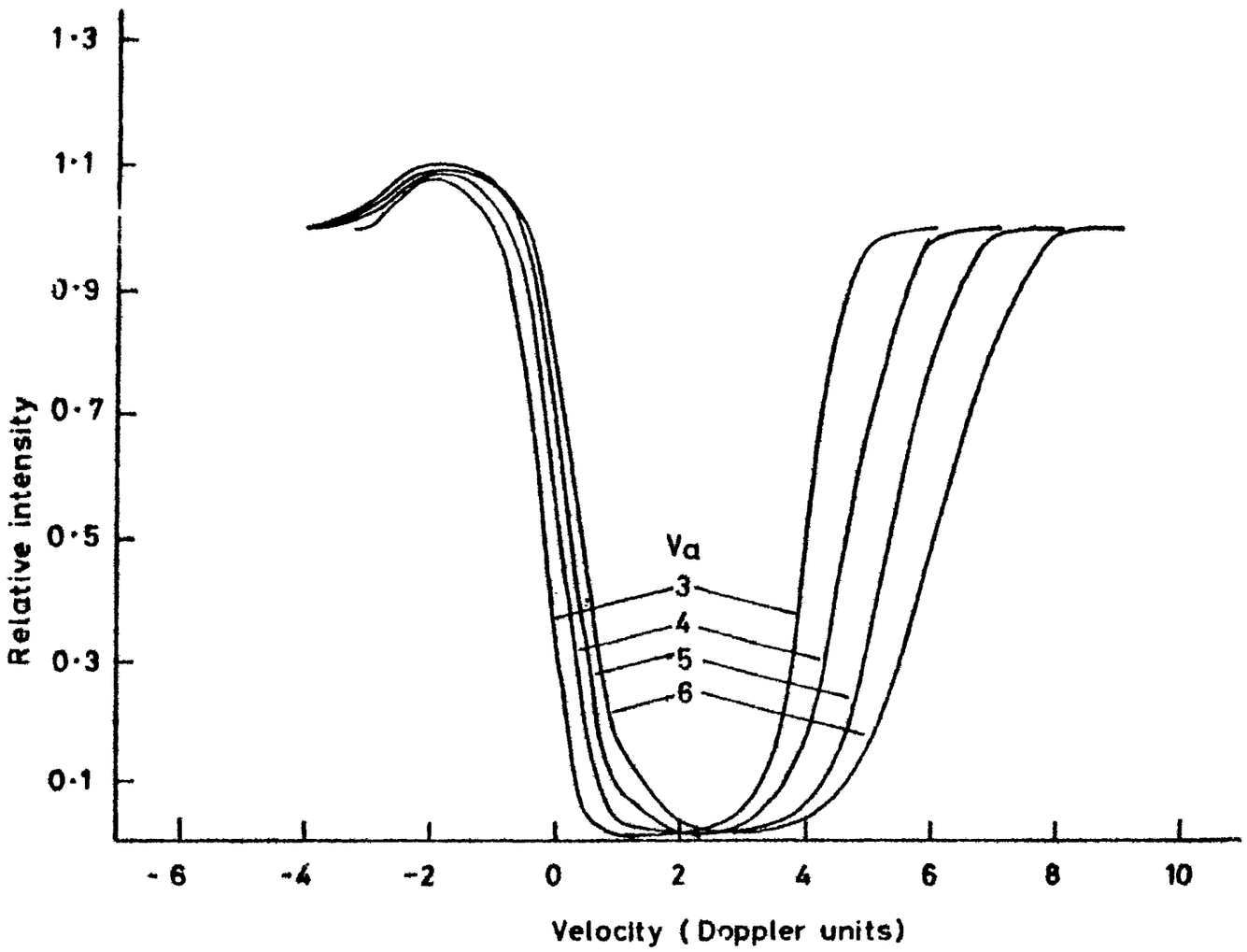

FIG. 14

Variation of case C computed profiles as a function of the inner velocity V_a labelled on each curve. The outer velocity $V_b = 2.0$, and $\tau = 3$.

Apart from the basic fact that a constant density in the envelope is highly unlikely, the computed line profiles for case A show that even for a relatively small optical depth, the line core is saturated. Since none of the observed lines are saturated, it was felt that this case may not represent the true physical situation.

Case B where $n(r) \propto 1/r^2$ and $V(r)$ = constant has been widely used by various workers in the study of CS envelopes. In the present analysis, this case was tried for various combinations of n_H and ΔR giving a wide coverage in integrated optical depth. In all cases, there is emission on the red side. The magnitude of the emission increases with higher optical depths. Although the bulk of the absorption occurs near the inner edge of the envelope, the total absorption of the line is low because of the rapid fall of density. With larger optical depth, the emission on the red side increases markedly but the EQW of the absorption line increases only marginally. Since the observed H_α EQW's are quite high and no strong red side emission is seen, this case was found unsuitable.

In the cases C and D, the density linearly decreases with radius. In the plane-parallel flow, velocity increases with radius while in the spherical case,

it decreases.

Since the inner velocity in case C is always higher than the outer velocity and since most of the absorbing material is located near the inner edge, the line core displacements are rather high. Further, it is found that to obtain EQW in the range of the observed EQW's, the velocity gradient has to be sufficiently large which in turn implies a large value of the inner velocity. However, Figure 4 shows no correlation between the observed EQW's and the line core displacements. Thus for no observed profile both the EQW and the line core displacement could be simultaneously matched with the computed series for this case.

The only choice then left was case D. Since in this case the inner velocity is always less than the outer velocity, the line core displacements are never very large. Moreover by increasing the integrated optical depth and choosing a suitable V_g, the EQW and the line core displacement could be matched.

It is to be emphasized that the sense of the velocity gradient is of crucial importance in obtaining this match. In a parallel study of the H_δ line in M giants, Boesgaard and Hagen (1979) have concluded that the H_α line forms in a rather narrow region of

increasing velocity gradient. The present computer analysis of the line profile for various density and velocity distribution has led us to the same conclusion.

In Table 6, the complete series of runs for case D are given. Also tabulated are the values of the line core displacement and the EQW's determined from the computed profiles.

To obtain the optical depth in the H_α line and the velocity field in the line forming regions of these stars, the following procedure was adopted.

It was found that the line core displacement for a given ξ_t and V_a was independent of the integrated optical depth and was linear function of V_b. From this correlation the outer velocity for a star can be determined from the observed line core displacement.

The EQW on the other hand was found to be a function of the optical depth and V_b. For a given EQW, a higher V_b corresponds to a lower integrated optical depth in the line. A plot was made of the computed EQW's as a function of integrated optical depth for a series of outer velocities for a given inner velocity and turbulence. Since the observed line core displacements fix the outer velocity independent of the optical depth,

Table 6

A : $V_a = 0.0$

R_{out} (10^{13} cm)	ξ_{st} (km/sec.)	Density n_H (cm^{-3})	τ	V_b (in thermal units)	ΔV (km/sec)	EQW (Å)
1.1	5	9.4×10^{10}	6	8.0	-10.5	0.95
				7.0	- 8.6	0.94
				6.0	- 9.5	0.87
				5.0	- 7.6	0.77
				4.0	- 9.5	0.78
				3.0	- 6.7	0.73
				2.0	- 5.7	0.65
				1.0	- 2.7	0.62
1.1		1.9×10^{11}	12	7.0	-14.3	1.19
				6.0	-13.4	1.11
				5.0	-12.4	1.08
				4.0	-11.5	0.93
				3.0	- 9.5	0.87
				2.0	- 7.6	0.76
				1.0	- 4.8	0.69
1.5		9.4×10^{10}	31	9.0	-28.6	1.80
				8.0	-28.6	1.69
				7.0	-25.8	1.57
				6.0	-23.9	1.52
				5.0	-23.9	1.28
				4.0	-17.2	1.17
				3.0	-14.3	1.07
				2.0	- 7.6	0.96
				1.0	- 4.8	0.86
1.1.		7.1×10^{11}	47	6.0	-28.6	1.41
				5.0	-22.9	1.32
				4.0	-17.2	1.18
				3.0	-16.2	1.05
				2.0	- 9.5	0.96
				1.0	- 3.8	0.87
1.1		9.4×10^{11}	62	6.0	-28.6	1.50
				5.0	-22.9	1.38
				4.0	-19.1	1.27
				3.0	-12.4	1.13
				2.0	- 9.5	1.02
				1.0	- 4.8	0.97

Table 6 continued

R_{out} (10^{13} cm)	ξ_t (km/sec.)	Density n_H (cm^{-3})	τ	V_b (in thermal units)	ΔV (km/sec)	EQW (Å)
1.1	10	1.3×10^{11}	6	8.0	-14.2	1.28
				7.0	-11.6	1.26
				6.0	-12.9	1.17
				5.0	-10.3	1.07
				4.0	-12.9	1.05
				3.0	- 9.0	0.98
				2.0	- 7.7	0.88
				1.0	- 3.9	0.83
1.1		2.6×10^{11}	12	7.0	-19.3	1.61
				6.0	-18.0	1.50
				5.0	-16.8	1.46
				4.0	-15.5	1.25
				3.0	-12.9	1.17
				2.0	-10.3	1.02
				1.0	- 6.4	0.93
1.5		1.3×10^{11}	31	9.0	-38.7	2.43
				8.0	-38.7	2.28
				7.0	-34.8	2.11
				6.0	-32.2	2.05
				5.0	-32.2	1.72
				4.0	-23.2	1.58
				3.0	-14.3	1.44
				2.0	-10.3	1.30
				1.0	- 6.4	1.16
1.1		9.8×10^{11}	47	6.0	-38.7	1.91
				5.0	-30.9	1.79
				4.0	-23.2	1.59
				3.0	-21.9	1.41
				2.0	-12.9	1.29
				1.0	- 5.2	1.18
1.1		1.3×10^{12}	62	6.0	-38.7	2.03
				5.0	-30.9	1.86
				4.0	-25.8	1.71
				3.0	-16.8	1.52
				2.0	-12.9	1.37
				1.0	- 6.4	1.30

Table 6 continued

R_{out} (10^{13} cm)	ξ_t (km/sec.)	Density n_H (cm^{-3})	τ	V_b (in thermal units)	ΔV (km/sec)	EQW (Å)
1.1	15	1.7×10^{11}	6	8.0	-18.8	1.75
				7.0	-15.4	1.72
				6.0	-17.1	1.60
				5.0	-13.7	1.46
				4.0	-17.1	1.40
				3.0	-11.9	1.34
				2.0	-10.2	1.20
				1.0	- 5.1	1.14
1.1		3.4×10^{11}	12	7.0	-25.6	2.19
				6.0	-23.9	2.04
				5.0	-22.2	1.99
				4.0	-20.5	1.70
				3.0	-17.1	1.59
				2.0	-13.7	1.39
				1.0	- 8.5	1.26
1.5		1.7×10^{11}	31	9.0	-51.2	3.31
				8.0	-51.2	3.10
				7.0	-46.1	2.88
				6.0	-42.7	2.79
				5.0	-42.7	2.35
				4.0	-30.7	2.15
				3.0	-25.6	1.96
				2.0	-13.7	1.77
				1.0	- 8.5	1.58
1.1		1.3×10^{12}	47	6.0	-51.2	2.60
				5.0	-40.9	2.43
				4.0	-30.7	2.16
				3.0	-29.0	1.92
				2.0	-17.1	1.76
				1.0	- 6.8	1.61
1.1		1.7×10^{12}	62	6.0	-51.2	2.76
				5.0	-40.9	2.53
				4.0	-30.7	2.33
				3.0	-22.2	2.07
				2.0	-17.1	1.87
				1.0	- 8.5	1.78

Table 6 continued

B : $V_a = 1.0$

R_{out} (10^{13} cm)	ξ_t (km/sec.)	Density n_H (cm^{-3})	τ	V_b (in thermal units)	ΔV (km/sec)	EQW (Å)
1.1	5	9.4×10^{10}	6	9.0	-19.1	1.00
				8.0	-17.2	0.92
				7.0	-18.1	0.89
				6.0	-17.2	0.82
				5.0	-14.3	0.78
				4.0	-14.3	0.70
				3.0	-13.4	0.67
				2.0	- 9.5	0.59
				1.0	- 6.7	0.58
		4.7×10^{11}	31	6.0	-28.6	1.26
				5.0	-23.9	1.13
				4.0	-19.1	1.05
				3.0	-16.2	0.96
				2.0	-12.4	0.87
				1.0	- 6.7	0.85
		9.4×10^{11}	62	6.0	-30.5	1.33
				5.0	-23.9	1.28
				4.0	-21.0	1.08
				3.0	-15.3	0.98
				2.0	-11.5	0.89
				1.0	- 9.5	0.91
	10	1.3×10^{11}	6	9.0	-25.8	1.35
				8.0	-23.2	1.24
				7.0	-24.5	1.20
				6.0	-23.2	1.11
				5.0	-19.3	
				4.0	-19.3	
				3.0	-18.0	
				2.0	-12.9	
				1.0	- 9.0	
		6.5×10^{11}	31	6.0	-38.7	1.70
				5.0	-32.2	1.52
				4.0	-25.8	1.41
				3.0	-21.9	1.30
				2.0	-16.8	1.18
				1.0	- 9.0	

Table 6 continued

R_{out} (10^{13} cm)	ξ_t (km/sec.)	Density n_H (cm^{-3})	τ	V_b (in thermal units)	ΔV (km/sec.)	EQW (Å)
1.1	10	1.3×10^{12}	62	6.0	-41.2	1.80
				5.0	-32.2	1.73
				4.0	-28.4	1.46
				3.0	-20.6	1.33
				2.0	-15.5	1.19
				1.0	-12.9	
	15	1.7×10^{11}	6	9.0	-34.1	1.84
				8.0	-30.7	1.69
				7.0	-32.4	1.66
				6.0	-30.7	1.51
				5.0	-25.6	1.44
				4.0	-25.6	1.29
				3.0	-23.9	1.23
				2.0	-17.1	1.09
				1.0	-11.9	1.06
		8.5×10^{11}	31	6.0	-51.2	2.31
				5.0	-42.7	2.07
				4.0	-34.1	1.92
				3.0	-29.0	1.77
				2.0	-22.2	1.61
				1.0	-11.9	
		1.7×10^{12}	62	6.0	-54.6	2.45
				5.0	-42.7	2.35
				4.0	-37.5	2.00
				3.0	-27.3	1.81
				2.0	-20.5	1.63
				1.0	-17.1	

the EQW- τ correlation for that outer velocity was used to determine τ corresponding to the observed EQW. Since the outer velocity in the computer runs were changed in steps of a Doppler unit, the fractional value of V_b determined from the first plot was rounded off to the nearest integer. The error involved in the optical depth so determined is minimal.

For very small optical depths ($\tau < 10$), the line core displacement outer velocity plot deviated significantly from the linear relation depicted in Figure 15. For these optical depths, the same line core displacement yields a very high outer velocity. Moreover, if this outer velocity were adopted, the observed EQW would give a much higher value of the optical depth than is implied by the first plot. Because of this inconsistency, deviations from the linear relation were ignored.

As shown in Table 6, the inner velocity was varied to obtain different series of computed profiles. With a higher inner velocity for the same outer velocity, the line core displacement is higher and the equivalent width is lower. This effect is enhanced with increasing inner velocity. Since many of the observed profiles showed high EQW for low line core displacements, the match with the above set of profiles was extremely poor.

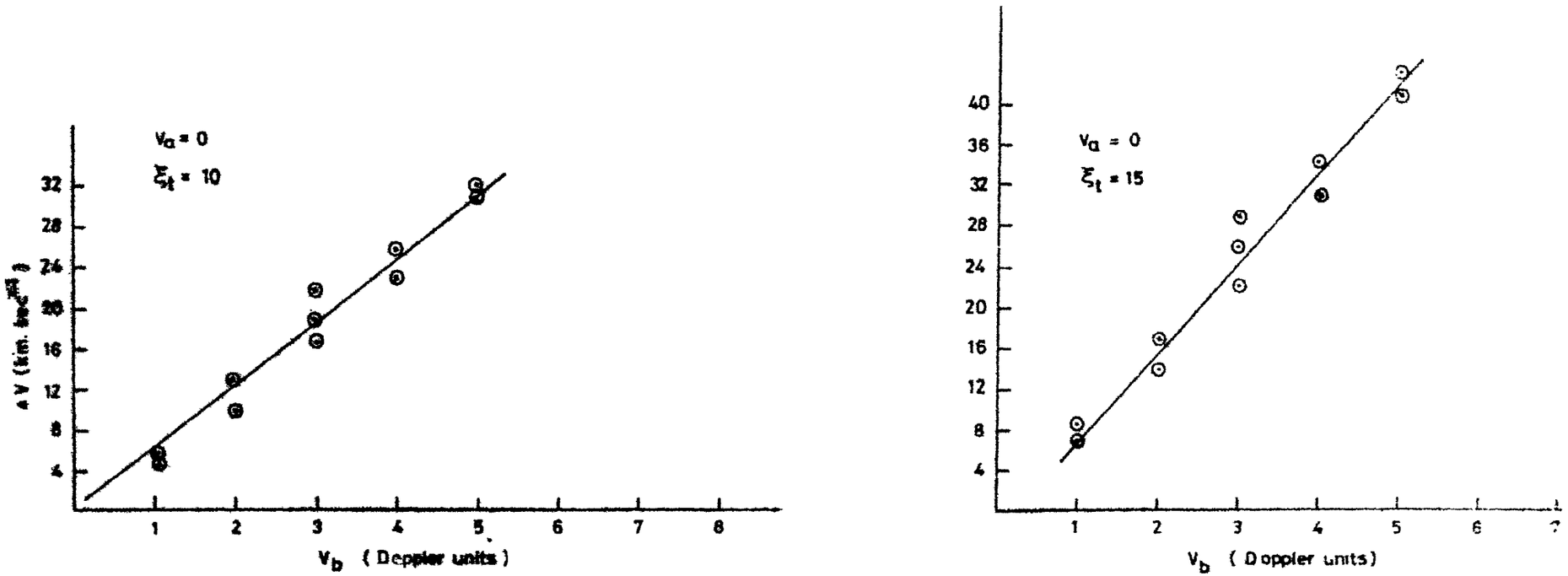

FIG. 15

Plot of the line core displacement ΔV in km sec^{-1} as a function of V_b in Doppler units for two turbulent velocities $\xi_t = 10$ km sec^{-1} and 15 km sec^{-1} in case D.

Only for three of stars HD 196093, HD 62576. amd JD 68553, having high line core displacements and relatively low EQW, a reasonable match was obtained. For these stars, the optical depths determined from this set of theoretical EQW-τ plot agreed reasonably well with the values determined from the $V_a = 0$ case.

d) Optical Depths and Column Densities.

In Table 7, τ the optical depth at the line center of H_α and V_{exp} the expansion velocity for each star derived from the above procedure for a given ξ_t and V_a are shown. The hydrogen column densities follow from equation (4.3) and are given in columns (3) and (6) in Table 7. The optical depths obtained are rather low (10-150) and consistent with the observation that the H_α line is unsaturated in these stars.

e) The Rate of Mass Loss

The rate of mass outflow from the atmosphere can be calculated from the steady state flow condition assuming spherical symmetry.

Using the equation

$$\frac{dM}{dt} = 4\pi r^2 \rho(r) V(r) \qquad \text{.. (4.9)}$$

Table 7

$V_a = 0.0$

Star	ξ_t = 10 km sec^{-1}				ξ_t =15 km sec^{-1}			
	τ	V_{exp} (km sec^1)	N_H (cm^2)	$\dot{M}$ ($M_\odot$ yr^{-1})	τ	V_{exp} (km sec^{-1})	N_H (cm^2)	$\dot{M}$ ($M_\odot$ yr^{-1})
HD 77912	132	12.89	1.52(+23)	8.76(-7)	60	14.93	9.15(+22)	6.11(-7)
ϵ Gem	165	8.06	1.90(+23)	6.84(-7)	88	9.81	1.34(+23)	5.88(-7)
33 Sgr	160	4.83	1.84(+23)	3.98(-7)	81	6.82	1.23(+23)	3.75(-7)
ζ Cep	152	14.50	1.75(+23)	1.13(-6)	76	15.35	1.16(+23)	7.96(-7)
HD 196093	68	19.34	7.83(+22)	6.77(-7)	28	19.62	4.27(+22)	3.74(-7)
ϵ Peg	165	8.70	1.90(+23)	7.39(-7)	89	11.52	1.36(+23)	7.00(-7)
η Per	170	7.41	1.96(+23)	6.49(-7)	93	9.38	1.40(+23)	5.87(-7)
HD 17958	73	17.72	8.40(+22)	6.65(-7)	13	18.34	1.98(+22)	1.62(-7)
9'CMa	111	6.77	1.28(+23)	3.87(-7)	51	8.53	7.62(+22)	2.91(-7)
41 Gem	112	9.35	1.29(+23)	5.39(-7)	60	11.09	8.99(+22)	4.46(-7)
HD 56577	113	5.80	1.30(+23)	3.37(-7)	52	7.68	7.77(+22)	2.67(-7)
HD 62576	88	15.47	1.01(+23)	6.98(-7)	30	16.63	4.57(+22)	3.40(-7)
HD 68553	59	31.26	6.79(+22)	9.48(-7)	27	30.71	4.12(+22)	5.66(-7)
HD 80108	115	21.91	1.32(+23)	1.29(-6)	47	22.18	7.16(+22)	7.10(-7)
HD 91056					95	10.66	1.45(+23)	6.91(-7)
β Ara	123	19.34	1.41(+23)	1.22(-6)	66	19.62	1.01(+23)	8.82(-7)
HD 4817	156	12.25	1.80(+23)	9.83(-7)	76	13.65	1.16(+23)	7.07(-7)
λ Vel	151	12.25	1.74(+23)	9.51(-7)	73	13.65	1.11(+23)	6.79(-7)
HD 89388	106	23.52	1.22(+23)	1.28(-6)	65	23.88	9.91(+22)	1.06(-6)
HD 137709	142	9.67	1.63(+23)	7.06(-6)	80	11.09	1.22(+23)	6.05(-7)
ζ Cyg					110	11.09	1.68(+23)	8.33(-7)
σ CMa	136	10.96	1.57(+23)	7.67(-7)	76	12.37	1.16(+23)	6.41(-7)
HD 216946	143	17.72	1.65(+23)	1.30(-6)	80	17.91	1.22(+23)	9.77(-7)

the mass-loss rate in the present model can be written as

$$\dot{M} = 4\pi m_H (1+\eta) V_{exp} N R_{in} \quad \text{.. (4.10)}$$

Where m_H is the mass of the hydrogen atom, η the relative abundance by weight of the elements heavier than hydrogen, N the hydrogen column density and R_{in} the inner radius of the model envelope. The value of η was adopted from Bell, Eriksson, Gustafsson and Nordlund (1976) and put equal to 0.42.

Using the values of column densities and expansion velocities from Table 7 in equation (4.10) $\dot{M}$ in $M_\odot$ Yr^{-1} was determined for all the programmes stars. Since the assumption of a particular value of ξ_t affects the value of the column density derived the mass-loss rate is slightly different in the two cases with ξ_t = 10 and 15 $kmsec^{-1}$. Since the Doppler unit of velocity is also dependent upon the choice of ξ_t there is a small dispersion (less than 2 $kmsec^{-1}$) in the derived values of V_{exp}. The mass loss rate $\dot{M}$ was plotted as a function of M_{bol} for the sixteen out of the twenty-three stars for which M_{bol} is available. Due to the small spread in M_{bol} for the stars chosen, there exists a narrow range in $\dot{M}$.

The values of $\dot{M}$ derived in the present work are a bit higher than what Reimers' (1975) empirical mass-loss relation implies. However, this relation is highly uncertain for G and K supergiants being based solely on Ca II data which display time variability. In most of the work on mass-loss so far hydrogen column densities were inferred rather than observed. This procedure has an inherent uncertainty, since the abundance of the metals in a particular star is not known a priori. In the present case the hydrogen column densities are directly obtained from the observations. Hence any uncertainty in the metal abundances does not affect the mass-loss rates.

f) Emission

For a number of stars small emission components were observed on the blue and red sides of the main absorption line. The blue emission was found to be more common than the emission in the red. For the computed profiles emission components on the red side are present whenever spherical flow is assumed. This is a direct consequence of radiative transfer calculations. However, the emission in the blue could never be reproduced with any of the assumed density and velocity distributions. This is left as an open question.

g) CaI] λ6573 line

Although a detailed analysis of the CaI] line has not been performed, the line profile computations do suggest an explanation for the strong correlation found between the line core displacements of CaI] and H_α . Since the CaI] line is expected to be of low optical depth, a medium expanding with the velocity implied by the H_α velocity shift would give a much lower line core displacement for this line. Although not conclusive, the correlation then indicates a co-extension of the CaI and H_α - regions.

The conclusions are discussed in the last Chapter.

CHAPTER V

Conclusions

The main conclusions of the present study are the following:

1. The observed asymmetry in the H_α line is a consequence of a net outward motion of the very outer layers of the atmosphere.

2. The present analysis confirms the origin of this line in a relatively small extent of the atmosphere with a fairly high density (10^{11}-10^{12} cm^{-3}), more characteristic of chromospheres than of CS envelopes.

3. The H_α line is of moderate optical thickness and is formed in a region of increasing velocity gradient. The column densities inferred are in the range of 10^{22}-10^{23} cm^{-2}.

4. The absence of correlation between the H_α EQW and the velocity shifts implies that the physical state of hydrogen is insensitive to the velocity field in the line forming region. On the other hand, the strength of the Ca II K line is well correlated to the corresponding velocity shift. This introduces

an additional uncertainty in the interpretation of Ca II observations because the dependence of the ionization state of Ca on the velocity field is not known. Therefore, the H_α line could be used as a more effective probe for the physical conditions of the lower chromosphere.

5. The rate of mass-loss derived from the column densities and expansion velocities of the observed G and K supergiants ranges between $1-11 \times 10^{-7}$ $M_\odot yr^{-1}$. The only other determination of mass-loss, in these stars is made on the basis of the shift of the chromospheric Ca II K emission. The derived rates are on the same order as obtained here.

6. The results obtained here are somewhat sensitive to the choice of the turbulent velocity ξ_t. In a detailed chromospheric model of α Boo (Ayres and Linsky 1975), a value of $\xi_t = 12.5$ kms^{-1} was found to fit the observations. There is no reason why G and K supergiants should have a lower ξ_t. The actual value of ξ_t in the H_α forming regions is difficult to obtain. However, within a reasonable range of values for ξ_t, the derived mass-loss rates differ by less than 50 per cent.

Although the H_α line has been studied in some detail, further improvement in the analysis may be achieved by solving the radiative transfer problem in a more elaborate fashion. In particular, since H_α in late-type stars is a photoelectrically controlled line, the effect of a continuum should be included in a full discussion of the line formation problem. Also the assumption of a 2-level atom model for the statistical equilibrium has to be verified by studying the Lyman-line formation in these atmospheres. The blue edge emission seen in a number of programme stars is yet to be explained by a rigorous theory.

On the observational side, higher resolution spectra of H_α would yield more detailed information on the expanding chromospheres of supergiants. The profile may then be studied.

The full potential of the spectra in the red has not yet been explored. In particular, the NaI D lines and the resonance lines of KI$\lambda\lambda$7665, 7699 should be investigated as probes for the extended envelopes of these stars. Sanner (1976) in his study of CS envelopes of M supergiants, used these lines to derive their physical properties.

A more detailed study of the CaI] line at 6573Å and the comparison with the CaII data is needed to obtain information on the state of Ca ionization.

Since the expansion velocities derived in the present study are in the range of -5 to -30 $kmsec^{-1}$, and since the velocity of escape from a supergiant (log g = 1-0) of $15M_{\odot}$ is on the order of 15 $kmsec^{-1}$, mass ejection is certainly taking place through the expanding chromospheres of many of these stars. However, what drives the mass-loss is not fully known although several theories have been proposed. Detailed studies of the kind described in the present work would help towards the elucidation of this problem.

REFERENCES

Adams, W.S., and McCormack, E. 1935, Astrophys. J., 81, 119.

Athay, R.G., and Thomas, R.N. 1958, Astrophys. J., 127, 96.

Ayres, T.R., and Linsky, J.L. 1975, Astrophys. J., 200, 660.

Bell, R.A., Eriksson, K., Gnstafason, B., and Nordlund, A. 1976, Astr. Ap. Suppl., 23, 37.

Bernat, A.P. 1977, Astrophys. J., 213, 756

Boesgaard, A.M., and Hagen, W. 1979, Astrophys. J., 231, 128.

Chaffee, F.H., Jr. and Schroeder, D.J. 1976, Ann. Rev. Astr. Ap., 14, 23.

Cohen, J. 1976, Astrophys. J., 203, L127.

Deutsch, A.J. 1956, Astrophys. J., 123, 210.

_____. 1960, in Stars and Stellar Systems, Vol.6, ed. J.L. Greenstein (Chicago, University of Chicago Press), P.543.

Dupree, A.K. 1976, in Physique dee Monvements dans lons Atmospheres Stellaires, Colloque International du C.N.R.S., ed. R. Cayrel et M. Steinberg, P.439.

Griffins, R.F. 1968, A Photometric Atlas of the spectrum of Arcturues, Cambridge Philosophical Society.

Groth, H.G., and Wellmann, P. 1970, Spectrum Formation in Stars with Steady-State Extended Atmospheres, IAU Colloquium No.2, NBS Special Publication 332.

Hagen, W. 1978. Astrophys. J. Suppl., 38, 1.

Hoffleit, D. 1964, Catalogue of Bright Stars, Yale University Observatory.

Hummer, D. 1962, Mon. Not. R. astr. Soc., 125, 21.

Humphreys, R.M. 1970, Astron. J., 75, 602.

Jager, C. de, and Neven, L. 1966, Bull. Astron. Inst. Neth., 18, 306.

Jefferies, J.T., and Thomas, R.N. 1959, Astrophys. J., 129, 401.

Johnson, H.L. 1966, Ann. Rev. Astr. Ap., 4, 193.

Keenan, P.C. 1978, in the HR Diagram, IAU Symposium No.80, ed. A.G. Davis Philip and D.S. Hayes, D. Reidel, P. 13.

Kraft, R., Preston, G.W., and Wolff, S.C. 1964, Astrophys. J., 140, 235.

Kuhi, L.V. 1974, in Highlights of Astronomy, Vol.3, 121.

Linsky, J.L., and Haisch, B.M. 1979, Astrophys. J., 229, L27.

Luck, R.E. 1977a, Astrophys. J., 212, 743.

_____. 1977b, Astrophys. J., 218, 752.

_____. 1978, Astrophys. J., 219, 148.

_____. 1979, Astrophys. J., 232, 797.

Mallia, B.A., and Pagel, B.E.J. 1978, Mon. Not. R. astr. Soc., 184, 35P.

McClintock, W., Henry, R.C., Moos, H.W., and Linsky, J.L. 1975, Astrophys. J., 202, 733.

Mihalas, D. 1978, Stellar Atmospheres (2nd Edition), Freeman.

Peraiah, A. 1978, Astr. Sp. Sci., 58, 189.

_____. 1979a, Astr. Sp. Sci., 63, 267.

_____. 1979b, private communication.

Reimers, D. 1973, Astr. Ap., 24, 79.

_____. 1975a, in Problemes d'Hydrodynamique Stellaire, 19th Liege International Astrophysical Colloquium, 8, P. 369.

Reimers,D. 1975b, in Problems in Stellar Atmospheres and Envelopes, ed. B. Baschek, W.H. Kegel and G. Traving (New York : Springer-Verlag), P. 229.

_____.1977a, Astr. Ap., 54, 485.

_____.1977b, ibid, 57, 395.

Saito, M. 1973, Astr. Sp. Sci., 22, 133.

Sanner, F. 1976, Astrophys. J. Suppl., 32, 115.

Thomas, R.N. 1957, Astrophys. J., 125, 260.

Warner, B. 1969, Mon. Not. R. Astr. Soc., 144, 333.

Weymann, R. 1962, Astrophys. J., 136, 844.

_____. 1963, Ann. Rev. Astr. Ap., 1, 97.

Wiese, W.L., Smith, M.W. and Glennon, B.M. 1966, Atomic Transition Probabilities, Vol.1.

Wilson, O.C., and Bappu, M.K.V. 1957, Astrophys. J., 125, 661.

Wilson, O.C. 1976, Astrophys. J., 205, 823.